LA-UR -91-2926

LA-UR--91-2926

DE92 000253

Los Alamos National Laboratory is operated by the University of California for the United States Department of Energy under contract W-7405-ENG-36

TITLE: THE RIDDLE OF HIGH-ENERGY BARYON NUMBER VIOLATION

AUTHOR(S): MICHAEL MATTIS, LANL, T-8, MS B285

SUBMITTED TO: PROCEEDINGS OF THE ICTP SUMMER SCHOOL IN HIGH ENERGY PHYSICS AND COSMOLOGY HELD IN TRIESTE, ITALY JULY 1-31, 1991.

DISCLAIMER

Los Alamos Los Alamos National Laboratory
Los Alamos, New Mexico 87545

LA-UR-91-xxxx

The Riddle of High-Energy Baryon Number Violation

MICHAEL P. MATTIS[†]

Theoretical Division T-8, Los Alamos National Laboratory
Los Alamos, NM 87545

The exciting possibility that anomalous baryon and lepton number violation might be observable at the next generation of supercolliders is suggested by an instanton calculation due to Ringwald and Espinosa. In these Lectures, the current controversial status of these claims is discussed, and several new technologies designed to analyze this question are reviewed. These technologies should contribute more generally to our understanding of weakly-coupled field theories in the nonperturbative regime where both energies and multiplicities are very large.

Lectures given at the ICTP Summer School in High Energy Physics and Cosmology, Trieste, 1991

September 1991

[†] Supported by a J. R. Oppenheimer Fellowship

Contents

1. INTRODUCTION

Two years back, a startling calculation by Ringwald[1] and later Espinosa[2] suggested the *possibility* that anomalous baryon and lepton number violation in the Standard Model *might* be observable at the upcoming generation of supercolliders. From the start, the reaction in the theoretical community has run the gamut from unbridled optimism to extreme skepticism, as can be seen in Table I. Today, theorists appear no closer to a consensus on this issue. However, a number of significant technical advances have been made which, in my view, have put almost within reach a definitive quantitative answer to the riddle of high-energy baryon number violation. The same methods will doubtless find other applications to open problems that fall under the general heading, What happens to weakly-coupled field theories when energies E and multiplicities $\langle n \rangle$ are very large, $E \sim m/g^2$ and $\langle n \rangle \sim 1/g^2$ where g and m are the coupling constant and typical particle mass of the theory?*

It is the purpose of these Lectures to illuminate the present state of the subject, starting with Ringwald's calculation and ranging through the most recent developments, in a way that emphasizes the essential ideas involved. In terms of level of detail I have attempted to navigate a middle course: on the one hand, back-of-the-envelope counting arguments are favored over rigorous derivations wherever possible; on the other hand, most of the calculations are presented in a sufficiently realistic manner that the motivated reader should be able to fill in the missing steps if so inclined. I should stress that the field is currently in a state of rapid flux so that these notes should be understood as "bulletins from the front." If a few of you are inspired hereby to join the fray, and contribute to the eventual solution of the riddle of high-energy baryon number violation, so much the better!

First, an apology. There are many possible paths to this subject, depending for instance on whether one prefers Euclidean to real-time methods, and whether one chooses to approach the critical energy scale m/g^2 (the 'sphaleron scale'[8]) from above or below. The reader will find a wide variety of approaches discussed in Ref. [9]. Here I will restrict myself to a specific path that starts with physics we believe we understand—instanton-mediated processes at low energies†—and confronts the corrections head-on as the energy is increased to the sphaleron. The goal is first to understand the taxonomy of Feynman graphs in instanton backgrounds that are relevant at sphaleron energies, and then to abstract the appropriate classical equations whose solutions implicitly sum up

* Related (and equally controversial) phenomena in scalar theories with no instantons are discussed in Refs. [3-7].

† I will assume that the reader understands this physics as well, at the level of Coleman's *Uses of Instantons*.[10]

these graphs. Certainly this is the approach that, to date, has been pushed the furthest; whether it will ultimately be viewed as the path of steepest descent for obtaining answers remains to be seen. Nor will I discuss the numerous quantum-mechanical toy models that have been advanced for gaining intuition about this subject, as in my opinion, the essential physics we are after depends crucially on the existence of an infinite number of modes and is therefore inescapably field-theoretic.[††]

These Lectures are organized as follows. In Sec. 2, the calculation of Ringwald and Espinosa is reviewed, and conflicting physical intuitions about its viability at sphaleron energies are presented. Dispersion relations are used to show that observable high-energy baryon number violation signals the breakdown of perturbation theory even for non-anomalous processes at *low* energies and multiplicities.

The heart of the Lectures is Secs. 3-5, which are devoted to the three classes of important corrections to Ringwald. (Here we will be brief, as individual overviews are given at the start of each of these Sections.) **Final-state corrections** are the topic of Sec. 3. At present, these are the best understood. They can be treated semiclassically, through the construct of distorted instantons. Numerically, they tame the rise of the anomalous cross section and ensure that the unitarity bound is not violated. But by themselves, they do not exclude the possibility of observable baryon number violation at a few times the sphaleron mass. **Multi-instanton corrections** (Sec. 4) become important, by definition, when the dilute instanton gas approximation breaks down. Whether this occurs *before* or *after* the one-instanton result has a chance to grow large is the key issue that will be discussed. Currently, this is an open question. Sec. 5 deals with the topic of **initial-state corrections** involving the high-energy incoming quanta. Unlike final-state corrections which are characterized by tree graphs and so can be treated semiclassically, initial-state corrections are

[††] One exception: an instructive and essentially solvable low-dimensional model discussed recently by Voloshin.[11]

Ken Aoki (10%) U.C.L.A.	Peter Arnold (10%) Argonne National Laboratory	Zvi Bern (.1%) Los Alamos National Lab
Kevin Cahill (0%) Univ. of New Mexico	James Cline ($e^{-2\pi/\alpha_W}$) Ohio State University	Mike Cornwall (10%) U.C.L.A
Michael Dugan (10%) M.I.T	Olivier Espinosa (50%) CALTECH	Glennys Farrar (e^{-2S_d}) Rutgers University
Haim Goldberg (10%) Northeastern University	Eduardo Guendelman (5%) Los Alamos National Lab.	Peter Herczeg (7%) Los Alamos National Lab.
Robert Jaffe (10^{-2}) M.I.T	David Kosower ($10^{-100\pm10}$) FERMILAB	Olaf Lechtenfeld (10^{-100}) City College, CUNY
Aneesh Manohar (10%) U. C. San Diego	Michael Mattis (5%) Los Alamos National Lab.	Pawel Mazur (10%) U.C.L.A
Larry McLerran (66.7%) Univ. of Minnesota	Emil Mottola (5%) Los Alamos National Lab.	Lev Okun (10%) ITEP
Stuart Raby (5%) Ohio State University	Andreas Ringwald (50%) DESY	Z. Ryzak (3.3%) Harvard University
E. V. Shuryak (10^{-1}) Brookhaven National Lab.	Arkady Vainshtein (30%) Univ. of Minnesota	John Vergados (1%) Univ. of Ioannina
M. Voloshin (90%) Univ. of Minnesota	Geoffrey West ($\mathcal{O}(\alpha)$%) Los Alamos National Lab.	Laurence Yaffe (1%) University of Washington

Table I. Participants in the Santa Fe Workshop on Baryon Number Violation at the SSC, April 1990 (Ref. 9). In parentheses is their answers to the question, What is the probability that baryon number violation might even in principle be observable in a supercollider? This poll was conducted by L. Okun.

dominated by graphs containing enormous numbers (order $1/g^2$) of loops. Nevertheless, we will review initial indications that these, too, admit a semiclassical treatment.

Indeed, if there is a tentative theme to these Lectures, it is that high-energy baryon number violation appears to be semiclassical from start to finish. This suggests the existence of a "master equation" that can in principle be solved *classically* on a computer, and whose solution will put the riddle to rest.

Acknowledgments. My own published work on this topic, plus many of the qualitative arguments contained in these notes, was done in collaboration with Peter Arnold. In addition, I have benefited from numerous conversations with most of the workers in this field, and am particularly indebted to Larry McLerran and Al Mueller for many patient explanations, particularly as regards the material of Sec. 5.

2. The Ringwald Surprise

2.1. A motivating paradox: sphaleron vs. instanton rate estimates

It has long been known that baryon and lepton number, B and L, are not strictly conserved by the weak interactions.[12] Because the $SU(2)$ gauge field* couples only to left-handed fermions, B and L are broken nonperturbatively by the Adler-Bell-Jackiw chiral anomaly.[13] Pictorially, the reason can be seen in fig. 1. Evidently the electroweak vacuum is not a unique state, but exhibits a periodic structure, labeled by integer values of $N_{\rm CS}$, the Chern-Simons or winding number of the $SU(2)$ gauge field. Explicitly, $N_{\rm CS}$ is given by

$$N_{\rm CS} \;=\; \frac{g^2}{16\pi^2}\int d^3\mathbf{x}\,\epsilon_{ijk}\left(A_i^a\partial_j A_k^a - \frac{g}{3}\epsilon_{abc}A_i^a A_j^b A_k^c\right)\,. \qquad (2.1)$$

Thanks to the anomaly, any transition between vacuum sectors is necessarily accompanied by a change in B and L:[12]

$$\Delta B \;=\; \Delta L \;=\; n_f \times \Delta N_{\rm CS} \;=\; -\frac{n_f\alpha_{\rm w}}{8\pi}\int_{t_1}^{t_2} d^4x\,\epsilon^{\mu\nu\alpha\beta}F_{\mu\nu}^a F_{\alpha\beta}^a\,, \qquad (2.2)$$

* We follow the practice in the field and set $\sin\theta_W = 0$ so that the gauge group is effectively pure $SU(2)_{\rm L}$.

where $\alpha_{\rm w} = g^2/4\pi \approx 1/32$, n_f is the number of families (henceforth three[14]), and $F_{\mu\nu}^a$ is the usual $SU(2)$ field strength.

Consider the following paradox. On the one hand, any transition between adjacent vacua can be viewed in Euclidean space as occurring entirely in the one-instanton sector of the theory. The Euclidean action along such a winding-number-changing path through configuration space is bounded from below by the instanton action[15,12] $2\pi/\alpha_{\rm w}$. So we expect a tiny suppression factor

$$e^{-4\pi/\alpha_{\rm w}} \;\approx\; e^{-400}$$

multiplying any B- and L-violating cross section, say for the quark-lepton process

$$q + q \;\rightarrow\; 7\bar{q} + 3\bar{l} \qquad (2.3)$$

which has $\Delta B = \Delta L = 3$ as the anomaly requires.† Moreover, this exponential suppression should apply not only at zero temperature but at finite temperatures as well; in this case the relevant Euclidean configurations are the periodic instantons, or 'calorons', discussed by Gross, Pisarski and Yaffe.[16,17]

On the other hand, when temperatures are of the order of the barrier height depicted in fig. 1, sufficiently early in the early universe, it should be the case that transitions between adjacent vacuum sectors happen all the time, and are adequately described by classical statistical mechanics.[18–20] The classical rate for such processes is governed by the Boltzmann factor $\exp(-E_{\rm sphal}/k_{\rm B}T)$; here $E_{\rm sphal}$ is the energy of Manton's gauge and Higgs saddle-point configuration known as the sphaleron[8] (from the Greek 'tending to fall') that corresponds to the top of the potential barrier in fig. 1. Dimensionally $E_{\rm sphal} \sim M_W/\alpha_{\rm w}$, while numerically $E_{\rm sphal} \sim 10$ TeV. When $k_{\rm B}T \sim E_{\rm sphal}$ the Boltzmann factor is of order unity and B and L violation should be unsuppressed. In fact, this happens at temperatures much *lower* than 10 TeV, since M_W itself, and hence the sphaleron mass, is temperature-dependent, vanishing above the symmetry-restoring phase transition at a few hundred GeV. In any case the paradox is

† Specifically, the fermion content of Eq. (2.3) must consist of one representative from each weak doublet.

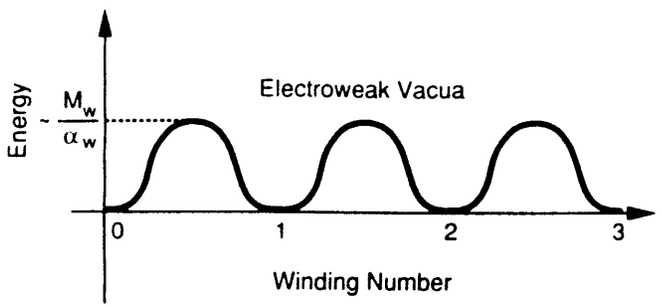

Fig. 1. The periodic structure of the Electroweak vacua. Transitions between adjacent vacua must be accompanied by a change of three units of B and L.

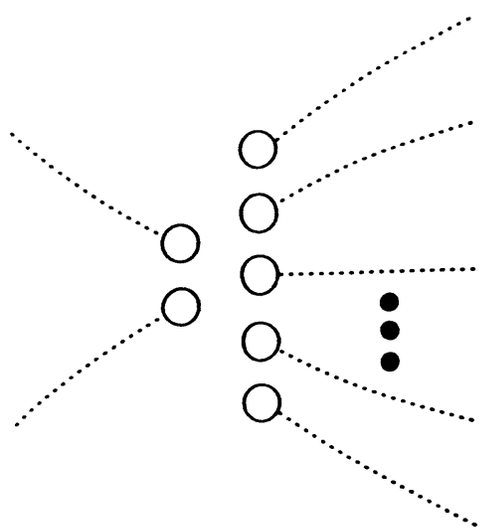

Fig. 2. A $2 \to n$ anomalous process in Ringwald-Espinosa approximation. Here and in all subsequent figures, a dotted line terminating in a circle stands for the substitution $\phi \to \phi_{\rm inst}$, where ϕ stands generically for all fields in the problem. (For fermions, $\phi_{\rm inst}$ means the zero mode of the Dirac operator in the instanton background.)

plain: *How can B-violating processes be suppressed (the instanton argument) and unsuppressed (the sphaleron argument) at the same time?*

This paradox motivated Ringwald to ponder much more complicated versions of the 'bare' B- and L-violating process (2.3) in which both the left- and right-hand sides are augmented by a large number, order $1/\alpha_w$, of soft ($p_T \sim M_W$) gauge and Higgs bosons as may be found in the finite-temperature heat bath. Loosely speaking, this is the particle content of the sphaleron. Ringwald conjectured that, at sufficiently high energies, the explicit instanton suppression $e^{-4\pi/\alpha_w}$ would be overcome by huge final-state phase space and initial-state flux factors, leaving an unsuppressed result. In this way the paradox between microscopic and macroscopic physics would be resolved in favor of the latter, *i.e.*, the sphaleron picture. But first, as a 'warm-up' problem, in order to postpone the complexity of a multi-particle initial state, Ringwald decided to focus on B- and L-violating processes in which the initial state was fixed at qq as in (2.3) while only the final-state multiplicity was allowed to grow large. *Surprisingly, he found the same phenomenon: an apparent transition to an unsuppressed rate.*

2.2. Estimating the B-violating cross section

The main elements of Ringwald[1] and Espinosa's[2] calculation are easily sketched. We are interested in the process

$$q + q \to 7\bar{q} + 3\bar{l} + n_w \times W + n_z \times Z + n_h \times \phi, \tag{2.4}$$

where n_w, n_z and n_h are the numbers of W's, Z's and Higgses created. Eventually we will want to construct the total inclusive B-violating cross section σ_B which entails summing over all values of $n_{W,Z,h}$ but for now we will hold these multiplicities fixed. Dropping the distinction between quarks and leptons and between W's and Z's for notational simplicity, one can write a Euclidean path integral for the Green's function corresponding to (2.4):

$$\mathcal{G}(x_1, \cdots, x_{12}, y_1, \cdots, y_{n_W+n_Z}, z_1, \cdots, z_{n_h}) =$$
$$\int (\mathcal{D}q)(\mathcal{D}W)(\mathcal{D}\phi) e^{-S_E} q(x_1) \cdots q(x_{12}) W(y_1) \cdots W(y_{n_W+n_Z}) \phi(z_1) \cdots \phi(z_{n_h}). \tag{2.5}$$

Here x_i, y_i and z_i give the positions of the fermions, W's and Higgses, respectively, and S_E is the Euclidean Weinberg-Salam action.

As stated earlier, $\mathcal{G}$ will only receive contributions from gauge configurations with unit winding number. The strength of these contributions can be estimated by performing a Gaussian expansion of S_E about the instanton. In the Weinberg-Salam model the instanton lives both in the gauge and in the Higgs field. Although no closed-form expression exists, in singular gauge it is known to have the following short- and long-distance asymptotics:[21]

$$\begin{aligned} (x-\xi)^2 \ll \rho^2: \qquad W^{\mu a}_{\rm inst}(x) &\simeq \frac{2\rho^2}{g} U_{ab} \frac{\bar\eta_{b\mu\nu}(x-\xi)_\nu}{(x-\xi)^2[(x-\xi)^2+\rho^2]}\ , \\ \phi_{\rm inst}(x) &\simeq v\left[\frac{(x-\xi)^2}{(x-\xi)^2+\rho^2}\right]^{1/2}\ . \end{aligned} \tag{2.6}$$

$$\begin{aligned} (x-\xi)^2 \gg \rho^2: \qquad W^{\mu a}_{\rm inst}(x) &\simeq -\frac{\rho^2}{g} U_{ab}\bar\eta_{b\mu\nu}\partial_\nu \frac{M_W}{r} K_1(rM_W)\ , \\ \phi_{\rm inst}(x) &\simeq v - \frac{v\rho^2}{2}\frac{M_{\rm higgs}}{r} K_1(rM_{\rm higgs})\ . \end{aligned} \tag{2.7}$$

Here v is the VEV of the Higgs, $\bar\eta_{a\mu\nu}$ is 't Hooft's symbol defined by[12]

$$\bar\eta_{aij} = \epsilon_{aij}, \quad \bar\eta_{a0i} = -\bar\eta_{ai0} = \delta_{ai}, \quad \bar\eta_{a00} = 0\ , \tag{2.8}$$

and ξ^μ, ρ and U denote the position, size and global weak isospin orientation of the instanton, respectively. (For antiinstantons, use $\eta_{a\mu\nu} \equiv (-)^{\delta_{\mu 0}+\delta_{\nu 0}}\bar\eta_{a\mu\nu}$.) The presence of a dimensionful parameter v means that, unlike in QCD, the instantons corresponding to different sizes ρ are not precisely degenerate. One finds that[12,21]

$$S_E[W_{\rm inst}(\rho), \phi_{\rm inst}(\rho)] \simeq \frac{2\pi}{\alpha_{\rm w}} + \pi^2\rho^2 v^2 \tag{2.9}$$

so that v serves as an infrared cutoff suppressing large instantons.

Now substitute

$$W(y_i) = W_{\rm inst}(y_i) + \delta W(y_i), \quad \phi(z_i) = \phi_{\rm inst}(z_i) + \delta\phi(z_i) \tag{2.10}$$

into Eq. (2.5). Ringwald and Espinosa's principal approximation consists of neglecting the fluctuation fields δW and $\delta\phi$ entirely, in the hope that they lead

to corrections of higher order in g. Similarly, replace the fermion fields $q(x_i)$ by the zero modes $q_0(x_i)$ of the Dirac operator in the instanton background.[12] In diagrammatic language, Ringwald's calculation of $\mathcal{G}$ is pictured in fig. 2. In this simple graph, each leg is merely replaced by the classical instanton value (zero mode, for fermions) of the relevant field.

Now that we have an approximate expression for $\mathcal{G}$, we calculate the cross section in the usual fashion. The first step is to extract an S-matrix element from $\mathcal{G}$. Fourier transforming the long-distance part of the fields, Eq. (2.7), to momentum space gives

$$\begin{aligned} W^{\mu a}_{\rm inst}(y_i) &\xrightarrow{\text{F.T.}} \frac{4i\pi^2\rho^2}{g} U_{ab}\frac{\bar\eta_{b\mu\nu}p_{i\nu}}{p_i^2+M_W^2} e^{ip_i\cdot\xi} + \cdots, \\ \phi_{\rm inst}(z_i) &\xrightarrow{\text{F.T.}} -\frac{2\pi^2\rho^2 v}{k_i^2+M_{\rm higgs}^2} e^{ik_i\cdot\xi} + \cdots\ , \end{aligned} \tag{2.11}$$

where the dots stand for terms nonsingular in momentum (including all short-distance contributions) as the Euclidean mass shell is approached, $p^2+M^2 \to 0$. There is a similar expression for the fermion zero modes $q_0(x_i)$ but we will be cavalier about the fermions for reasons we will justify later on. The S matrix is formed by analytically continuing $\mathcal{G}$ to real-time and amputating the external legs according to the LSZ prescription. The net result is that each gauge and Higgs leg contributes a residue of $-4i\pi^2\rho^2 g^{-1}U_{ab}\bar\eta_{b\mu\nu}p_{i\nu}e^{-ip_i\cdot\xi}$ and $2\pi^2\rho^2 v e^{-ik_i\cdot\xi}$, respectively, where the rotation to Minkowski space of all vector quantities is understood, *e.g.*, $W^0 \to iW^0$ and $p^0 \to ip^0$.

We are not quite done constructing the S matrix, as the instanton's collective coordinates ξ, ρ and U still need to be integrated over. The ξ integration is trivial and enforces overall momentum conservation, setting the sum $\sum k_i$ of final-state momenta equal to the initial momentum $P_{\rm tot}$. Unfortunately, the rest of the calculation is complicated by a rash of Lorentz and isospin indices, and so, purely for pedagogical purposes, let us forget temporarily about the gauge particles as well as the fermions and focus exclusively on the scalar Higgs. In

this case there is no U integration to be performed, while the ρ integration is simply

$$\int_0^\infty \mathcal{D}\rho \left(2\pi^2\rho^2 v\right)^{n_h} e^{-2\pi/\alpha_w - \pi^2\rho^2 v^2} \sim n_h! \left(\frac{2}{v}\right)^{n_h} e^{-2\pi/\alpha_w}. \tag{2.12}$$

The cross-section for fixed n_h is obtained by squaring the S matrix element (2.12), multiplying by the volume of phase space

$$\mathcal{T}_{n_h} = \left[\prod_{i=1}^{n_h} \int \frac{d^3\mathbf{k}_i}{(2\pi)^3 2\omega_{\mathbf{k}_i}}\right] (2\pi)^4 \delta^4(\textstyle\sum k_j - P_{\rm tot}) \,, \tag{2.13}$$

and dividing by $n_h!$ for identical particles as well as by the initial-state flux factor. A back-of-the-envelope estimate for $\mathcal{T}_{n_h}$ for large n_h can be had by assuming equipartition of energy together with the relativistic approximation $\omega_{\mathbf{k}} = |\mathbf{k}|$. In the center-of-mass frame $P_{\rm tot} = (E, \mathbf{0})$ this gives

$$\begin{aligned} \mathcal{T}_{n_h} &\sim \frac{1}{E^4}\left(\int_0^{E/n_h} \text{const.} \times |\mathbf{k}|\, d|\mathbf{k}|\right)^{n_h} \\ &= \frac{1}{E^4}\left(\frac{\text{const.} \times E^2}{n_h^2}\right)^{n_h} \approx \frac{1}{E^4}\frac{(\text{const.} \times E^2)^{n_h}}{(n_h!)^2} \end{aligned} \tag{2.14}$$

using Stirling's formula.* Assembling the various pieces and dropping overall factors gives

$$\sigma_{n_h}(E) \sim e^{-4\pi/\alpha_w} \frac{1}{n_h!}\left(\frac{\text{const.} \times E^2}{v^2}\right)^{n_h} . \tag{2.15}$$

The important point, first observed by McLerran, Vainshtein and Voloshin,[22] is that this expression exponentiates when summed on n_h, giving for the total inclusive B-violating cross section in this Higgs-only example,

$$\sigma_{\rm higgs}(E) \sim e^{-4\pi/\alpha_w}\, e^{\text{const.} \times E^2/v^2} = \exp\left\{\frac{4\pi}{\alpha_w}\left[-1 + \text{const.} \times \left(\frac{E}{E_{\rm sphal}}\right)^2\right]\right\} \tag{2.16}$$

since $E_{\rm sphal} \sim v/g$.

* This crude estimate does not give the constant in (2.14) correctly; we will do a better job in Sec. 3.3 below.

Taken at face value, Eq. (2.16) implies that the tunneling suppression $e^{-4\pi/\alpha_w}$ is completely canceled at high energies, $E \sim E_{\rm sphal}$, due to the enormity of phase space. Of course, as Ringwald and Espinosa both acknowledged, this expression *cannot* be taken at face value at high energy; for one thing, when $E > E_{\rm sphal}$ it violates the unitarity bound in a most spectacular way. In the following Sections we will discuss systematically the range of validity of Ringwald's calculation, but already at this stage we can identify one potential problem, albeit one that can be easily remedied,[23] namely the relativistic approximation $\omega_{\mathbf{k}} = |\mathbf{k}|$ made in Eq. (2.14). This is justified so long as the average energy per final-state particle is large, $E/\langle n_h\rangle \gg M_{\rm higgs}$. But (2.15) implies for the average multiplicity,

$$\langle n_h\rangle \sim \alpha_w^{-1}(E/E_{\rm sphal})^2 \tag{2.17}$$

so that the relativistic approximation is only valid when $E \ll E_{\rm sphal} \times (M_W/M_{\rm higgs})$.† This unusual feature—that the problem becomes *less* relativistic as the energy *increases* to the sphaleron—is due to the remarkable rise in final-state multiplicity. Conversely, our use of Stirling's approximation to the factorial only makes sense if $\langle n_h\rangle \gg 1$, that is, $E \gg M_W/g$ using (2.17).

What happens if we focus on W and Z production instead of Higgs production? At a crude level (neglecting the index mess) the calculation outlined above changes in two essential ways. First, the residue that appears in parentheses in the integral of Eq. (2.12) is now proportional to ρ^2/g instead of $\rho^2 v$ so that the right-hand side of (2.12) should be replaced by $n_W!(\text{const.} \times g v^2)^{-n_W} e^{-2\pi/\alpha_w}$. Note that the dominant contribution to the integral comes from instantons of size

$$\langle\rho\rangle \sim \frac{\sqrt{n_W}}{\pi v} . \tag{2.18}$$

Second, in the phase-space estimate (2.14), the integrands should be proportional to $|\mathbf{k}|^3$ instead of $|\mathbf{k}|$ due to the k_μ's that appear in the residue

† From now on we will treat the unknown ratio $M_W/M_{\rm higgs}$ as a number of order unity, that is $\lambda \sim \alpha_w$, in order to avoid the complications of an additional small parameter in the problem.

of $W_{\rm inst}$, and consequently the right-hand side of (2.14) now scales like $(\text{const.} \times E^4)^{n_W}/(n_W!)^4$. Remembering the $1/n_W!$ for indistinguishable particles and making use of Stirling's formula once again, one estimates

$$\begin{aligned}\sigma_{\rm gauge}(E) &\sim e^{-4\pi/\alpha_w} \sum_{n_W} \frac{1}{(n_W!)^3} \left(\frac{\text{const.} \times E^4}{g^2 v^4}\right)^{n_W} \\ &\sim e^{-4\pi/\alpha_w} \sum_{n_W} \frac{1}{(3n_W)!} \left(\frac{\text{const.} \times E^{4/3}}{g^{2/3} v^{4/3}}\right)^{3n_W} \\ &= \exp\left\{\frac{4\pi}{\alpha_w}\left[-1 + \text{const.} \times \left(\frac{E}{E_{\rm sphal}}\right)^{4/3}\right]\right\}\end{aligned} \tag{2.19}$$

for $E \ll E_{\rm sphal}$. The faster-rising function of energy in the exponent compared to Eq. (2.16) means that at low energies (when B violation is certainly exponentially tiny) it is W and Z production, and not Higgs production, that dominates the B-violating final state:

$$\langle n_W \rangle \sim \alpha_w^{-1} (E/E_{\rm sphal})^{4/3}, \quad E \ll E_{\rm sphal}\,. \tag{2.20}$$

Eq. (2.20) can only be valid so long as $\langle n_W \rangle \gg 1$, that is $E \gg M_W/\sqrt{g}$. Finally, if one allows *both* Higgs and gauge production, which is the problem we are really interested in, then at the naive level of the above derivation one finds Eqs. (2.17)-(2.20) confirmed once again.

Ironically, in the above discussion we have completely ignored the primary fermions that are directly responsible for the B and L violation. The justification is that unlike the bosons, whose number grows rapidly with energy, their number is fixed at twelve by the anomaly. As a result they do not affect the exponent of (2.19), but only give a *sub*exponential contribution to the anomalous cross section, on a par with many other contributions that we have been dropping all along, such as instanton determinants, or the running of the coupling constant.[12] Nor, as we shall see in Sec. 3.3 below, does fermion-antifermion pair production contribute to this exponent. What we are after, in other words, is not the full anomalous cross section $\sigma_{\not B}$, a hopeless task, but rather its *leading exponential behavior*, defined as $\left(\frac{\alpha_w}{4\pi}\right) \log \sigma_{\not B}$ in the limit $\alpha_w \to 0$ with $E/E_{\rm sphal}$ fixed (the so-called "holy grail function" to be discussed in Sec. 3.1).

Experimentally, the primary fermions produced by the process (2.4) would be difficult to identify. Instead, the signatures of anomalous B violation would be (a) the enormous number of gauge and Higgs bosons produced, and (b) the sudden turn-on of the B-violating cross section as a function of parton energy. But until it is understood whether or not such processes are suppressed by 100 orders of magnitude, further phenomenological speculation is surely premature.

2.3. Observations on the Ringwald result: Minkowski-continued instantons, pointlike behavior, pessimistic vs. optimistic physical pictures

Some comments on the above calculation are in order. Perhaps the most basic point, emphasized by Ringwald, is that the instanton or pseudoparticle can also serve as a *bona fide* particle, in the field-theoretic sense that when continued to Minkowski space, its Fourier transform (2.11) has an isolated pole on the mass shell. A useful if unfamiliar construct to keep in mind throughout these Lectures is that of a *Minkowski-continued* instanton, which is simply the Wick rotation $x_0 \to ix_0$, $x^2 \to -x^2 + i\epsilon$ of the usual Euclidean instanton. While these objects have no evident topological meaning, working directly with Minkowski-continued instantons is a convenient shorthand for working in Euclidean space with ordinary instantons, then rotating the amplitudes back to Minkowski space where the LSZ amputation procedure is defined. We will see later (Sec. 3.6) that the reason Minkowski-continued instantons have mass-shell poles is due to their structural similarity with Feynman propagators $G_F(x,\xi)$, ξ being the instanton's position.

How to explain the rapid initial growth in the B-violating cross section? Mathematically, the reason is easy to discern.[22] Look again at the form of the Higgs component of the instanton in momentum space, Eq. (2.11). Upon LSZ amputation, each Higgs contributes a momentum-independent constant, namely $2\pi^2\rho^2 v$, to the amplitude. (The phases $e^{ik_i\cdot\xi}$ just enforces overall momentum conservation when ξ is integrated over, so forget about them.) Therefore, *on shell*, the instanton acts like an elementary multiparticle vertex at which n_h Higgs lines meet. The absence of momentum dependence means that this vertex is pointlike, with no form factors to suppress high momentum transfer.

A pointlike n_h-point vertex with $n_h \sim 1/\alpha_w$ is highly nonrenormalizable, and like the old nonrenormalizable 4-Fermi theory of the weak interactions, leads to a rapid growth in the cross section which violates the bounds imposed by unitarity if extrapolated to sufficiently high energies. We have made this argument only for Higgs production but a similar albeit more complicated argument is available for gauge particles as well; at any rate the "Higgs-only" cross section is a *lower bound* on the total B-violating cross section.

The pointlike on-shell behavior of amplitudes is an inevitable consequence of the $O(4)$ symmetry of the instanton.[24] And so it was originally believed that if a *distorted* instanton were used instead, one with lower symmetry, the growth of $\sigma_{\not B}$ would be sharply curtailed, and $\sigma_{\not B}$ would remain exponentially tiny. Yet that is not necessarily true! Indeed, a particular class of distorted instantons, where the distortion is due to the back-reaction of only the *final-state* particles on the instanton, will be discussed in Secs. 3.4-3.5 below.[25–27] It will be seen that despite the lower symmetry, $O(3)$ instead of $O(4)$, $\sigma_{\not B}$ in this approximation *still* grows observably large at energies on the order of 40 TeV,[27] out of reach of the SSC but nevertheless formally of order E_{sphal}.

Thus, in the event that B violation turns out to be exponentially suppressed even at several times the sphaleron energy, the initial-state quanta must play an essential damping role. What does physical intuition suggest in this regard? The answer is, it depends on one's physical picture of what are the essential configurations that dominate $\sigma_{\not B}$. We outline two contrasting physical pictures below:

The pessimistic picture. As the old saying goes, "You can't make a fish in a $p\bar{p}$ collider" (fig. 3). The basic reason is that a fish is a heavy extended object whose spatial extent is much greater than its Compton wavelength. It therefore consists of a very large number of soft quanta, each one of which should cost roughly a factor of α to produce. Now suppose that one conceives of high-energy B-violation as happening primarily via sphaleron production:

$$\text{2 hard initial quanta} \longrightarrow \text{sphaleron} \longrightarrow \frac{\pi}{\alpha_w}\ \text{soft final quanta}\,. \tag{2.21}$$

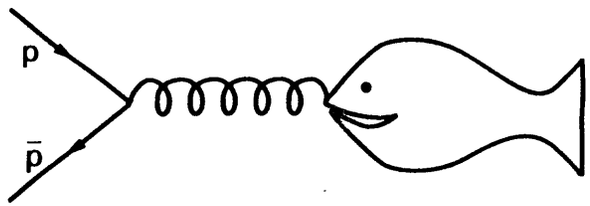

Fig. 3. "You can't make a fish in a $p\bar{p}$ collider."

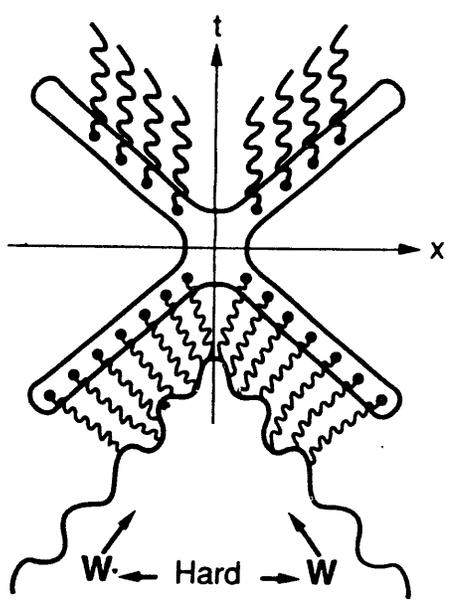

Fig. 4. A schematic picture of how two hard incoming particles can give up their energy to a Minkowski-continued instanton. Each vertex factor of g from a peripheral emission is compensated by a g^{-1} gained back when the emitted quantum is absorbed by the instanton. The instanton then spits out a large number of soft final-state quanta into the forward light cone.

Like a fish, a sphaleron is a heavy static extended object; it is localized to a region $\sim M_W^{-1} \gg E_{\rm sphal}^{-1}$ and comprises order π/α_w soft gauge and Higgs bosons. Producing such a configuration should therefore cost approximately π/α_w factors of α_w. So if this picture is right, one expects

$$\sigma_{\not B} \sim \sigma(2 \to \text{sphaleron}) \sim (\alpha_w)^{\pi/\alpha_w} \sim \exp\left(-\frac{\pi}{\alpha_w}\log\frac{1}{\alpha_w}\right) , \qquad (2.22)$$

which is in the same ballpark as the 't Hooft suppression $e^{-4\pi/\alpha_w}$. That is to say, the process can never happen. A more sophisticated analysis encapsulating this basic physics can be found in Ref. [28].

The optimistic picture. In contrast, suppose that the relevant configuration is not a sphaleron at all, but rather is more like an instanton. Unlike sphalerons, instantons are localized in Euclidean, not Minkowski space. This distinction has dramatic consequences, for as we saw, an instanton interacts with physical quanta in its Minkowskian incarnation, which is not a localized object, but has support all along the light cone (fig. 4). That means that the high-energy incoming quanta have a long time and large distance in which to lose their energy to the instanton. There is then no obvious reason why anomalous processes cannot take place.

The typical length scales involved can be estimated using a simple argument due to Li, McLerran, Voloshin and Wang.[29] These authors would have us consider the full renormalized propagator $G(p,q)$ in the Minkowski-continued instanton background, where p and q are the initial-state momenta. By Lorentz invariance,

$$G(p,q) = G(p^2, q^2, p\cdot q) , \qquad (2.23)$$

ignoring the overall factors which carry the requisite Lorentz and isospin indices. We are interested in on-shell or nearly on-shell processes as the energy gets very large,

$$p^2 \sim m^2, \quad q^2 \sim m^2, \quad p\cdot q \sim E^2 \gg m^2 . \qquad (2.24)$$

Let us work in the center of mass frame with $\mathbf{p}$ and $\mathbf{q}$ aligned along the z axis. In lightcone coordinates defined by

$$k^\pm \equiv k_0 \pm k_3 , \qquad (2.25)$$

the large components of p and q are then p^+ and q^- which are order E, while the small components are p^- and q^+ of order m^2/E. The position-space propagator is $G(x^2, y^2, x\cdot y)$. Elementary notions of Fourier transforms then implies

$$x^\pm \sim 1/p^\mp , \quad y^\pm \sim 1/q^\mp \qquad (2.26)$$

so that, as in multiperipheral scattering, the characteristic distances probed by the propagator are of order

$$(x-y)^2 = (x^+ - y^+)(x^- - y^-) \sim -x^+y^- \sim -E^2/m^4 , \qquad (2.27)$$

which is huge! In this picture, the short-distance structure of the instanton is never probed at all.

2.4. Dispersion relations, and goodbye perturbation theory

Another type of argument that drives home the dramatic consequences of observable B violation at high energies comes from the use of dispersion relations.[4,5] In general, dispersion relations relate the high-energy and low-energy domains of a theory. For example, under very general assumptions, a forward ($t=0$) elastic $2 \to 2$ scattering amplitude $\mathcal{A}$ for a self-conjugate scalar field such as Higgs is expected to satisfy*

$$\mathcal{A}(s, t=0) = \text{poles} + \frac{1}{\pi}\int_{4m^2}^{\infty} ds' \left(\frac{1}{s'-s} + \frac{1}{s'+s-4m^2}\right) \text{Im}\,\mathcal{A}(s', t=0) , \qquad (2.28)$$

the two terms in parentheses arising from the s- and u-channel cuts, respectively. In turn, $\text{Im}\mathcal{A}(s', t=0)$ is related to the total anomalous-plus-nonanomalous cross section $\sigma_{\rm tot}(s')$ by the optical theorem.

---

* If $\mathcal{A}$ falls off too slowly at large s for purposes of closing contours, one constructs a dispersion relation instead for the quantity $\mathcal{A}/s^p$ for some positive power p; the conclusions are the same. What follows is a variant of an argument given by Zakharov.[5]

Now let us suppose that $\sigma_{tot}(s')$ receives a large (that is, not exponentially suppressed) nonperturbative anomalous contribution above the sphaleron scale. A simple model of such a contribution, suggested by H. Goldberg, is

$$\sigma_{anom}(s') \sim m^{-2}(m^2/s')^k \alpha^l \theta(s' - \text{const.} \times m^2/\alpha^2) , \qquad (2.29)$$

where k and l are some small powers, $k, l \ll 1/\alpha$. Through the dispersion relation (2.28), this in turn will affect $\mathcal{A}$ starting at some low order** in α (in this example, at order α^{2k+l-2}). We emphasize that this low-order contribution to $\mathcal{A}$ will *not* be calculable perturbatively, that is through the Feynman diagrams of the theory, since the perturbative part of $\text{Im}\mathcal{A}$ is entirely given by the perturbative part of σ_{tot} through Cutkosky's cutting rules.[30]

From a theoretical point of view, the apparent conclusion is disturbing. *If* in a weakly coupled theory anomalous processes such as B violation grow large at the sphaleron scale, then one of the following must be true: either perturbation theory breaks down at some low order—even as applied to *non*anomalous physics at *low* energies and *low* multiplicities such as elastic scattering—or, alternatively, dispersion relations themselves are invalid, and the entire analytic structure of amplitudes in field theory must be rethought. By itself, this line of reasoning does not rule out the possibility that Ringwald's process becomes large at high energies (although it may exclude analogous phenomena in Borel-summable theories[5]); but surely it raises the stakes.

We now leave such indirect arguments behind, and begin the explicit analysis of corrections to the Ringwald result.

** For purposes of this discussion, "low order" can mean, say, α^{10}, which might never be ruled out experimentally, but still signals a much earlier formal breakdown of perturbation theory than the $1/\alpha$ order expected on general grounds for asymptotic series.

3. Final-State Corrections

This Section is devoted to the first corrections to Ringwald's calculation that come in as the energy is increased toward the sphaleron, namely the final-state corrections.[31–35] Although these corrections are most easily pictured as Feynman diagrams in the instanton background, such as fig. 5, the resulting perturbation series is disastrously behaved already at energies far below the sphaleron, with successive terms actually *larger* than the preceding ones[33,34] (Sec. 3.1). More sophisticated resummation techniques are required. Two such resummations, the R-term method due to Khlebnikov, Rubakov and Tinyakov[35] (Secs. 3.2-3.3) and the valley method advocated by Khoze and Ringwald[26] (Sec. 3.5) are reviewed. The two methods, which can be formally equated to one another by means of the optical theorem[36] (Sec. 3.6), are naturally interpreted in terms of *distorted* instantons[25] (Sec. 3.4), where the distortion is caused by the backreaction of the enormous number of produced particles on the ordinary zero-energy instanton. The new "small parameter" employed by these methods turns out to be $(E/E_{sphal})^{2/3}$ in the Weinberg-Salam model.[35] Thus they can be trusted at least up to some finite fraction of the sphaleron energy—a vast improvement over naive perturbation theory. Whether they can be trusted for energies extending up to and beyond E_{sphal} is not presently known, and depends on delicate issues of analytic continuation.

The tentative moral of this Section will be seen in fig. 17 below, namely: final-state corrections alone do not refute the initial indication that B violation becomes unsuppressed at high energies; they serve only to unitarize the growth of the cross section.[27]

3.1. Breakdown of perturbation theory: a specific example, a general scaling argument, final-state trees, and the holy grail function

To understand the disastrous behavior of naive perturbation theory in a concrete example, consider the simple diagrammatic correction to fig. 2 illustrated in fig. 6. In this figure, four of the final-state Higgs have been tied together using the $\lambda\phi^4$ piece of the action. More accurately, this interaction

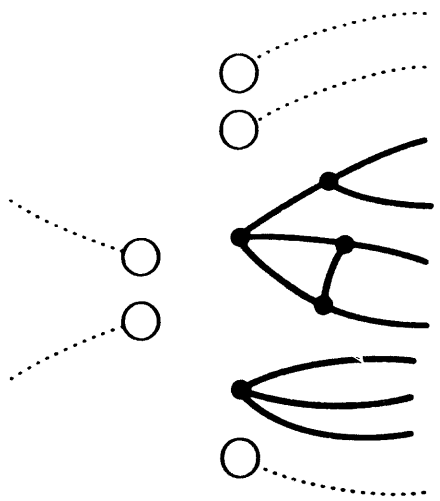

Fig. 5. A typical final-state correction in a $2 \to n$ process. Solid lines are propagators in instanton backgrounds, dotted lines were defined in fig. 2.

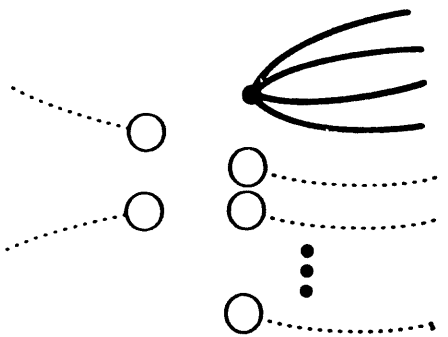

Fig. 6. A simple final-state correction in which four of the final-state Higgs have been tied together using the $\lambda(\delta\phi)^4$ vertex, while all other quanta are treated in Ringwald-Espinosa approximation.

can be written as $\lambda(\phi_{\rm inst} + \delta\phi)^4$, dividing the scalar field into 'classical' and 'quantum' parts as per Eq. (2.10), and it is the $\lambda(\delta\phi)^4$ piece ignored by Ringwald that is being used.

Of course, such an interaction wholly among final-state particles is forbidden by energy conservation at the vertex if free propagators are used, *i.e.*, in the zero-instanton sector of the theory. But in the present case the propagators are those in the instanton background,[37,38] as shown in fig. 7. Since at this stage of the calculation the instanton is viewed as having a *fixed* position ξ, such propagators do not conserve energy-momentum.

Let us estimate on the back of an envelope the relative strength of fig. 6 compared to the Ringwald contribution where the four interacting Higgs are simply replaced by $\phi_{\rm inst}$.[33] Whereas the Ringwald result for these lines is proportional to four powers of the Higgs mass-shell residue $\rho^2 v$, the interaction part of fig. 6 can only depend on some power of ρ. This is because in the relativistic regime when $E/\langle n_h \rangle \gg M_{\rm higgs}$, ρ is the only dimensionful parameter appearing in the Schwinger-Dyson equation for the propagator in the instanton background.[37,32] Dimensional analysis then gives ρ^4. In addition, there is an explicit factor of λ from the vertex. Finally, there is a combinatoric factor of $\binom{n_h}{4} \sim n_h^4$ that counts the number of independent ways that this interaction can be inserted amongst the final-state Higgs lines. In sum, fig. 6 is responsible for a multiplicative correction to the Ringwald result that scales like $\lambda\rho^4(\rho^2 v)^{-4} n_h^4$. Using the scaling relations (2.17), (2.18) and (2.20) together with the simplifying assumption $\lambda \sim \alpha_{\rm w}$ used earlier, this quickly translates to $\alpha_{\rm w}^{-1}(E/E_{\rm sphal})^{16/3}$.

The important point here is not the precise exponent 16/3, which depends on what diagram we are looking at, but rather the observation that when $E \sim E_{\rm sphal}$, this supposedly perturbative correction to Ringwald's calculation is actually *bigger* by a factor of $1/\alpha_{\rm w}$. The situation is even worse when one accounts for *multiple*, *disconnected* insertions of the $\lambda(\delta\phi)^4$ interaction into the final state that occur ostensibly at higher order in perturbation theory. Two insertions give a correction of order $1/\alpha_{\rm w}^2$, three insertions give $1/\alpha_{\rm w}^3$, and so forth. By standard combinatoric arguments, such corrections sum up when

$n_h \gg 1$ to give an exponentially important multiplicative correction of the form $\exp\left[\frac{\pm\text{const.}}{\alpha_w}(E/E_{\text{sphal}})^{10/3}\right]$.

We have worked through this one diagrammatic example at some length to illustrate the bedeviling consequences of the scaling relations (2.17), (2.18) and (2.20). Of course, on a graph-by-graph basis this line of reasoning quickly becomes cumbersome. Fortunately, there is a general argument that determines the size of all final-state corrections at the sphaleron energy.[33] To this end, let us rescale all fields and coordinates in the problem as follows:

$$x \to \bar{x} = gvx, \qquad W(x) \to v\bar{W}(\bar{x}), \qquad \phi(x) \to v\bar{\phi}(\bar{x}), \qquad q(x) \to g^{\frac{1}{2}}v^{\frac{3}{2}}\bar{q}(\bar{x}). \tag{3.1}$$

This can be thought of as a product of two rescalings, the first being the usual redefinition of fields often used in instanton problems to bring a factor of $1/g^2$ out in front of the action, and the second removing the engineering dimensions from all fields and coordinates, measured in units of $2M_W = vg$. Ignoring Yukawa couplings, the action in terms of the dimensionless rescaled fields is

$$S_E = \frac{1}{g^2}\int d^4\bar{x}\,\bar{\mathcal{L}}_E\left[\bar{W}(\bar{x}),\bar{\phi}(\bar{x}),\bar{q}(\bar{x});\lambda/g^2\right]. \tag{3.2}$$

The only parameters are λ/g^2 and an overall factor of $1/g^2$. Now consider expanding the action about the instanton. The action of the small fluctuations $\delta\bar{A}$ and $\delta\bar{\phi}$ will depend on ρ, giving

$$\delta^2 S_E = \frac{1}{g^2}\int d^4\bar{x}\,\delta^2\bar{\mathcal{L}}_E\left[\delta\bar{W}(\bar{x}),\delta\bar{\phi}(\bar{x}),\bar{q}(\bar{x});\lambda/g^2,gv\rho\right]. \tag{3.3}$$

The rescaled instanton size $gv\rho$ has entered as a third parameter.

What does (3.3) imply at the sphaleron energy? From (2.18) and (2.20) if follows that $gv\rho \sim 1$. The analysis is particularly simple if we assume as before that $\lambda \sim g^2$, as then the only dependence of (3.3) on parameters is the overall factor of $1/g^2$. (The argument also goes through for the case $\lambda \ll g^2$ if one treats the self-interaction and mass of $\delta\phi$ as a small perturbation and ignores them in what follows.) Counting powers of g^2 is now equivalent to counting powers of $\hbar$. Thus, connected graphs with j external $\delta\bar{\phi}$ legs, k external $\delta\bar{W}$

legs and l loops behave as $g^{2(j+k+l-1)}$. The contribution of such a graph to the $(n_h + n_w)$-point Green's function $\left\langle(\delta\bar{\phi})^j(\bar{\phi}_{\text{inst}})^{n_h-j}(\delta\bar{W})^k(\bar{W}_{\text{inst}})^{n_w-k}\right\rangle$ is therefore $g^{2(j+k+l-1)}$ times smaller than the Ringwald-Espinosa approximation $\left\langle(\bar{\phi}_{\text{inst}})^{n_h}(\bar{W}_{\text{inst}})^{n_w}\right\rangle$, which is of order one when expressed in terms of rescaled fields. However, for $j \ll n_h$ and $k \ll n_w$, the combinatoric enhancement due to the number of ways to choose which external fields to take as $\delta\bar{\phi}$ or $\delta\bar{W}$ and which as $\bar{\phi}_{\text{inst}}$ or $\bar{W}_{\text{inst}}$ is of order $n_h^j \times n_w^k \sim g^{-2(j+k)}$. So, at the sphaleron, the graph gives a multiplicative correction of order $g^{2(l-1)}$; for trees this $\sim 1/\alpha_w$.

Of course, in general the graph will also contain functional dependence on the scalar products $\bar{p}_i \cdot \bar{p}_j$ of the rescaled final-state momenta, $\bar{p}_i \equiv p_i/gv$, but these do not alter the g counting since at the sphaleron, $p_i \sim E/\langle n_{h,w}\rangle \sim gv$ and so the $\bar{p}_i \cdot \bar{p}_j$ are all just numbers of order unity.* Moreover, since the p_i's lie in the forward light cone, the quantities $\bar{p}_i \cdot \bar{p}_j$ are all positive; consequently, functions that depend on them tend to add coherently when summed over all combinatoric possibilities, rather than random-walk-cancel.

It follows that *all* connected tree graphs give multiplicative corrections of order $1/\alpha_w$ at the sphaleron.[33–35] As before, this result exponentiates when the disconnected tree graphs are accounted for. We conclude that, if all the tree-graph final-state corrections could be evaluated, they would modify the low-energy Ringwald result (2.19) to read[33–35]

$$\sigma_{\not B} \sim \exp\left(\frac{4\pi}{\alpha_w}F_{hg}(E/E_{\text{sphal}})\right) \tag{3.4}$$

where the function F_{hg} (the subscript stands for 'holy grail') depends in a complicated way on the ratio λ/α_w. In contrast, final-state loop graphs only give subexponential contributions to $\sigma_{\not B}$. At low energies $F_{hg} \approx -1$ and we recover the usual 't Hooft suppression.[12] The key question before us is: *Does*

* This last argument breaks down when one of the $\bar{p}_i$'s is a high-energy initial-state line, and indeed, we will see explicitly in Sec. 5 that when initial lines are involved, loop graphs are important.[39–40]

the holy grail function F_{hg} climb close enough to zero that B-violation might be observable at accessible energies?

To begin to answer this question, let us admit the following: the fact that an infinite number of final-state tree graphs need to be evaluated suggests that we have been expanding about the *wrong instanton*. Finding the right instanton is the goal we now work toward.

3.2. The R-term method of Khlebnikov, Rubakov and Tinyakov in the zero-instanton sector

In the Ringwald scenario outlined in Sec. 2, the instanton tunneling suppression is potentially compensated by an enormous factor due largely to phase space. Clearly, it is desirable to have a formalism in which these two effects are treated on the same footing from the outset, that is to say, a formalism in which phase space appears in the exponent of the path integral as a term in a generalized 'action'. The R-term method of Khlebnikov, Rubakov and Tinyakov is just such a formalism.[35]

The following simple derivation of the R-term is due to Larry McLerran. Forget about instantons for the moment, and consider the Green's function

$$\int \mathcal{D}\phi\, e^{iS[\phi]}\phi^*(p_1)\phi^*(p_2)\phi(k_1)\cdots\phi(k_n) \qquad (3.5)$$

where $p_{1,2}$ are the initial-state and k_i the final-state momenta, and ϕ is a generic scalar field (for simplicity) with action

$$S[\phi] = \int d^4x \left(\tfrac{1}{2}(\partial_\mu\phi)^2 - \tfrac{1}{2}m^2\phi^2 - V(\phi)\right) . \qquad (3.6)$$

As always with momentum-space Green's functions, the overall momentum-conserving δ-function is implicit in (3.5) and never needs to be written out. The total inclusive 2 →any cross section $\sigma_{\rm tot}$ is constructed in the usual textbook fashion, by amputating the external legs, squaring, integrating over phase space

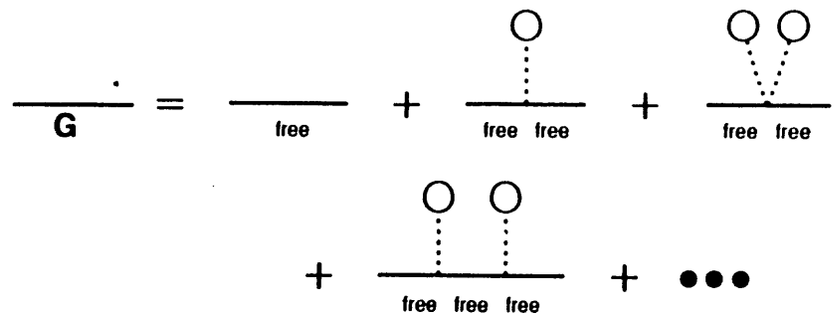

Fig. 7. Definition of a tree-level propagator G in the instanton background. Appropriate Fadeev-Popov constraints must also be specified; see Sec. 5.1.

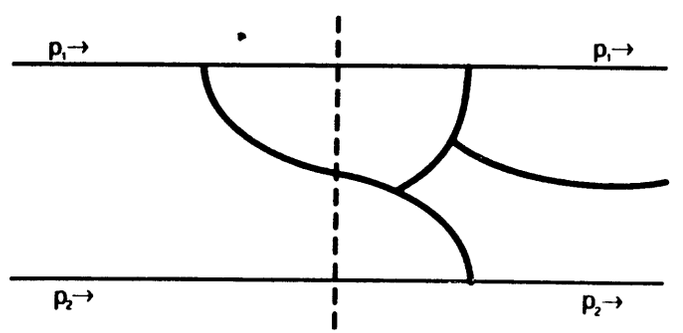

Fig. 8. A typical R-term graph in the perturbative sector of the theory. See text for Feynman rules. The dashed line stands for the operator $\hat{R}$, Eq. 3.10.

and summing on n. These steps are accomplished *all at once* in the double path integral expression

$$\sigma_{\rm tot} = \frac{1}{F}\lim_{p_1^2\to m^2}(p_1^2-m^2)^2\lim_{p_2^2\to m^2}(p_2^2-m^2)^2 \times\sum_{n=0}^{\infty}\frac{1}{n!}\prod_{i=1}^{n}\int\frac{d^4k_i}{(2\pi)^3}\delta(k_i^2-m^2)\theta(k_{i0})(k_i^2-m^2)^2\int\mathcal{D}\phi\int\mathcal{D}\phi' e^{iS[\phi]}e^{-iS[\phi']} \times\phi^*(p_1)\phi'(p_1)\phi^*(p_2)\phi'(p_2)\phi(k_1)\phi'^*(k_1)\cdots\phi(k_n)\phi'^*(k_n) \tag{3.7}$$

where F is the usual flux factor. The key observation is that thanks to the $1/n!$ for identical final-state particles, the sum on n exponentiates. Defining the bilinear 'residue field'

$$R(k) = \lim_{k^2\to m^2}(k^2-m^2)^2\phi(k)\phi'^*(k)\,, \tag{3.8}$$

one arrives at the compact expression[35]

$$\sigma_{\rm tot}\sim\frac{1}{F}\int\mathcal{D}\phi\int\mathcal{D}\phi'\,R^*(p_1)R^*(p_2)\;\times \exp\Big(iS[\phi]-iS[\phi']+\int\frac{d^4k}{(2\pi)^3}\delta(k^2-m^2)\theta(k_0)R(k)\Big)\,. \tag{3.9}$$

The third term in the exponent, the phase space integral, is the R-term of Khlebnikov, Rubakov and Tinyakov. For later convenience, we introduce the Hilbert-space operator $\hat{\rm R}$ defined by its Minkowski-space matrix elements,

$$\zeta\hat{\rm R}\psi=\int\frac{d^4k}{(2\pi)^3}\delta(k^2-m^2)\theta(k_0)(k^2-m^2)\zeta(-k)\cdot(k^2-m^2)\psi(k)\,. \tag{3.10}$$

The R-term in (3.9) can then be written even more compactly as $\phi'^*\hat{\rm R}\phi$.

Before turning to instanton physics, let us understand what the R-term means in the familiar context of perturbation theory in the vacuum sector.[41] Think of the three terms in the exponent of (3.9) as defining a generalized 'action' of some sort. Eq. (3.9) then implies that an amputated 4-point Green's function generated by this 'action' reproduces the 2 →any cross section in the

original theory. A formal expression for such a 4-point function is obtained by traditional functional methods.[42] First, couple ϕ and ϕ' to external sources:

$$S[\phi]\;\to\;S[\phi]+\int d^4x\,J(x)\phi(x)\,,\qquad S[\phi']\;\to\;S[\phi']+\int d^4x\,J'(x)\phi'(x)\,. \tag{3.11}$$

The 4-point function we want is the amputated version of

$$\frac{\delta}{\delta J(p_1)}\frac{\delta}{\delta J(p_2)}\frac{\delta}{\delta J'(-p_1)}\frac{\delta}{\delta J'(-p_2)}e^{-i\int d^4x\,V\left(-i\delta/\delta J(x)\right)}e^{i\int d^4x\,V\left(i\delta/\delta J'(x)\right)} \times\int\mathcal{D}\phi\int\mathcal{D}\phi'\,\exp\Big\{\int d^4x\big(\tfrac{i}{2}[(\partial_\mu\phi)^2-m^2\phi^2]-\tfrac{i}{2}[(\partial_\mu\phi')^2-m^2\phi'^2] +i\phi J-i\phi'J'\big)+\int\frac{d^4k}{(2\pi)^3}\delta(k^2-m^2)\theta(k_0)(k^2-m^2)^2\phi(k)\phi'(-k)\Big\}\,, \tag{3.12}$$

with the understanding that after the functional differentiation is performed, $J(x)$ and $J'(x)$ are to be set to zero. Since the potentials $V(\phi)$ and $V(\phi')$ have been pulled out as derivatives, the remaining exponent is Gaussian in ϕ and ϕ', so that the double path integration can be carried out in closed form. A little algebra gives

$$\frac{\delta}{\delta J(p_1)}\frac{\delta}{\delta J(p_2)}\frac{\delta}{\delta J'(-p_1)}\frac{\delta}{\delta J'(-p_2)}e^{-i\int d^4x\,V\left(-i\delta/\delta J(x)\right)}e^{i\int d^4x\,V\left(i\delta/\delta J'(x)\right)}\;\times \exp\Big\{\int\frac{d^4k}{(2\pi)^4}\Big(i\tfrac{J(k)J(-k)}{k^2-m^2+i\epsilon}-i\tfrac{J'(k)J'(-k)}{k^2-m^2-i\epsilon}+2\pi J(k)J'(-k)\delta(k^2-m^2)\theta(k_0)\Big)\Big\}\,. \tag{3.13}$$

From the argument of this exponential, one reads off the propagators of the theory, which evidently come in three flavors. As an illustration of this admittedly peculiar diagrammatics, a typical 'R-term graph' generated by the generalized 'action' is shown in fig. 8. The Feynman rules are as follows. Propagators to the left of the dashed line come from the first term in the exponential and have the usual form $i(k^2-m^2+i\epsilon)^{-1}$. Propagators to the right of the dashed line have the complex conjugated value $-i(k^2-m^2-i\epsilon)^{-1}$ as given by the second term in the exponential. Finally, propagators that cross the dashed line are $2\pi\delta(k^2-m^2)\theta(k_0)$, from the JJ' term of (3.13), and so serve to put the propagating quanta on shell and ensures that energy flows consistently from left to right. It is this propagator that can be traced to the R-term of Eq. (3.9).

We now recognize the role of the R-term in the zero-instanton sector: it serves as an elegant bookkeeping device for implementing the cutting rules of the optical theorem.[30]

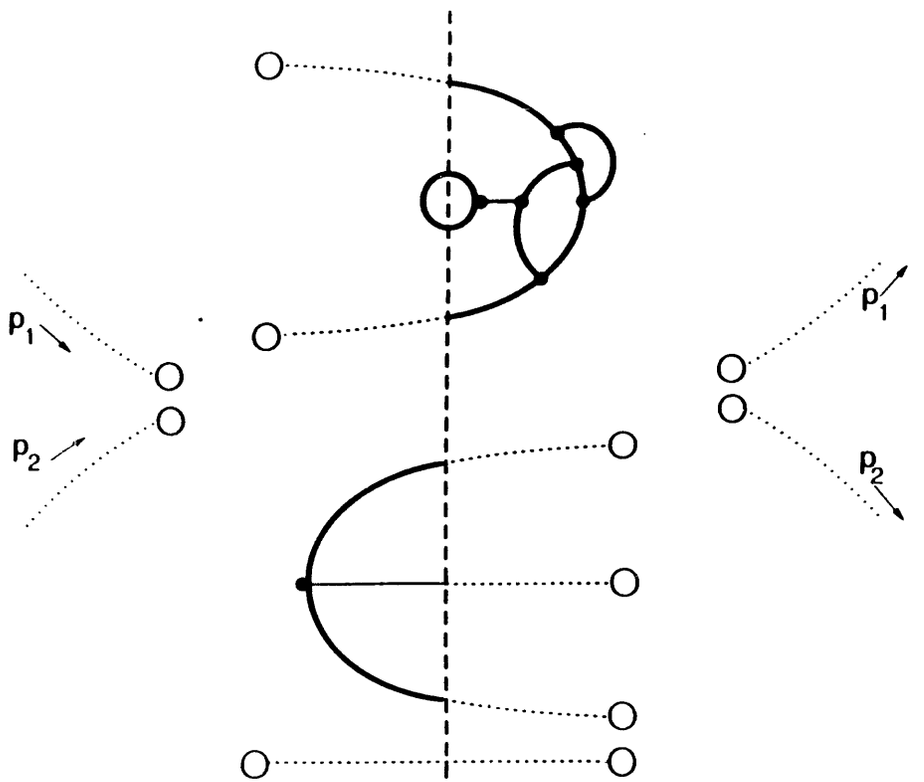

Fig. 9. A typical R-term graph in the instanton sector of the theory. See text for Feynman rules.

3.3. The R-term method in the one-instanton sector

The true usefulness of the R-term, however, lies in semiclassical problems such as B violation, in which the presence of phase space in the exponent is ideally suited to steepest descent, as we shall soon see. Let us return to Eq. (3.9), where now for convenience ϕ and ϕ' stand for both gauge and Higgs fields but are restricted to the one-instanton sector of the theory. As in Eq. (2.10) we write

$$\phi(x) = \phi_{\rm inst}(x;\xi,\rho,U) + \delta\phi(x), \quad \phi'(x) = \phi_{\rm inst}(x;\xi',\rho',U') + \delta\phi'(x)\,, \quad (3.14)$$

splitting the fields into 'classical' and 'quantum' pieces, and explicitly indicating the position, size and isospin orientation of the instantons. On the other hand, since in this Section we are focusing exclusively on final-state corrections, we will continue to make the naive Ringwald-Espinosa replacement $\phi(x) \to \phi_{\rm inst}(x;\xi,\rho,U)$ and $\phi'(x) \to \phi_{\rm inst}(x;\xi',\rho',U')$ for the *initial*-state quanta that comprise $R^*(p_1)R^*(p_2)$ in (3.9). It is useful to factor out of the double path integral the independent collective coordinate integrations over (ξ,ρ,U) and (ξ',ρ',U') and to postpone these till the end of the calculation. Following Ref. [35], these will be carried out in steepest descent approximation.

Treating the R-term as a term in a generalized 'action' as before, we see that the Feynman graphs generated by the double path integral are of the type illustrated in fig. 9. Unlike fig. 8, lines in fig. 9 that lie to the left of the dashed line are not free propagators, but rather propagators in the $\phi_{\rm inst}(x;\xi,\rho,U)$ background[37,38] (fig. 7) continued to Minkowski space. Lines that lie to the right of the dashed line are Minkowski-continued propagators in the background of $\phi_{\rm inst}(x;\xi',\rho',U')$, with opposite $i\epsilon$ prescriptions. The dashed line itself stands for LSZ amputation and phase-space integration as embodied by the R-term; for gauge particles, a projection onto physical polarizations is also understood. Dotted lines ending in circles are instantons, as always.

The diagrammatics is further simplified if one refrains from drawing the two incoming and two outgoing instanton lines which are common to all such graphs when one restricts attention to final-state corrections. The remaining parts of

the diagrams are given by the exponential of *connected* graphs, examples of which are pictured in figs. 10-15. In these figures, the distinction has been restored between gauge and Higgs particles, which are indicated by wavy and straight lines, respectively.

Consider the first of these graphs, fig. 10. As per our Feynman rules, this represents the product of $W_{\rm inst}(k;\xi,\rho,U)$ with $W^*_{\rm inst}(k;\xi',\rho',U')$, where each is rotated to Minkowski space, amputated and summed over physical polarizations, and then phase space is integrated over. The source of this graph is easily seen from Eq. (3.9). It comes straight from the R-term, with $R(k)$ given in (3.8), and where only the classical pieces of the gauge fields are chosen. We expect from the discussion in Sec. 2 leading up to Eq. (2.19) that fig. 10 is responsible for the $(E/E_{\rm sphal})^{4/3}$ contribution to the holy grail function F_{hg}. Let us review how this comes about in the approach of Khlebnikov, Rubakov and Tinyakov.[35] Here we will go into a little more detail than elsewhere in these Lectures, in order to give an accurate flavor of the types of calculations that have been done.

The gauge field residues can be read off from Eq. (2.11). Evaluating fig. 10 then gives

$$\left(\frac{-4i\pi^2\rho^2}{g}\right)\left(\frac{4i\pi^2\rho'^2}{g}\right)\int\frac{d^4k}{(2\pi)^3}\delta(k^2-M_W^2)\theta(k_0)e^{ik\cdot\Delta\xi}\sum_{abc}\Pi_{ab}(\mathbf{k})U'^{\dagger}_{bc}U_{ca}\ . \tag{3.15}$$

Here $\Delta\xi = \xi' - \xi$, and Π_{ab} is the polarization sum

$$\Pi_{ab}(\mathbf{k}) = \sum_m \epsilon^m_\mu(\mathbf{k})\bar\eta_{a\mu\nu}k_\nu\epsilon^{m*}_\alpha(\mathbf{k})\bar\eta_{b\alpha\beta}k^*_\beta\ , \tag{3.16}$$

with $k_\nu = (i\omega_{\mathbf{k}},\mathbf{k})$. We anticipate that after the collective coordinate integrations are performed, U' will equal U at the saddle point by symmetry arguments, so that $U'^{\dagger}U$ in (3.15) can be replaced by δ_{ab}.* The resulting $\bar\eta$ identity is given

* A technical aside: actually it is possible to carry out the U integration exactly, instead of in saddle-point approximation as in Ref. [35]. The reason is that $\Pi_{ab}(\mathbf{k})$ and $(U'^{\dagger}U)_{ta}$ can be written, respectively, as $\delta_{ab}(\omega^2_{\mathbf{k}}+\mathbf{k}^2)-2k_ak_b+2i\epsilon_{abc}\omega_{\mathbf{k}}k_c$ and $\delta_{ab}(a_0^2-\mathbf{a}^2)+2a_aa_b+2\epsilon_{abc}a_0a_c$ with $a_0^2+\mathbf{a}^2=1$. So if one simultaneously rotates $\Delta\vec\xi$ and $\mathbf{k}$ to imaginary values keeping $k\cdot\Delta\xi$ fixed, the a_μ can simply be absorbed into a redefinition of k_μ, after which $\Delta\vec\xi$ and $\mathbf{k}$ can be rotated back.

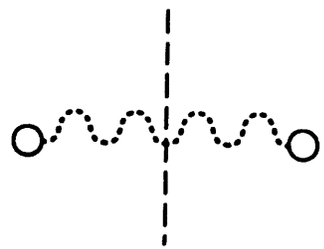

Fig. 10. The leading-order connected subgraph in the R-term approach, which contributes to the holy grail function F_{hg} at the 4/3 order. The two wavy dotted lines are $W_{\rm inst}$ and $W'^*_{\rm inst}$.

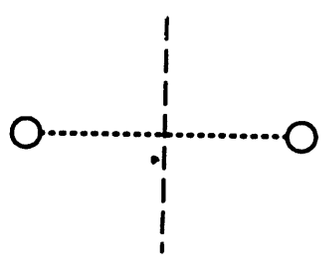

Fig. 11. Same as fig. 10 for the Higgs. This graph contributes to F_{hg} at the 6/3 order.

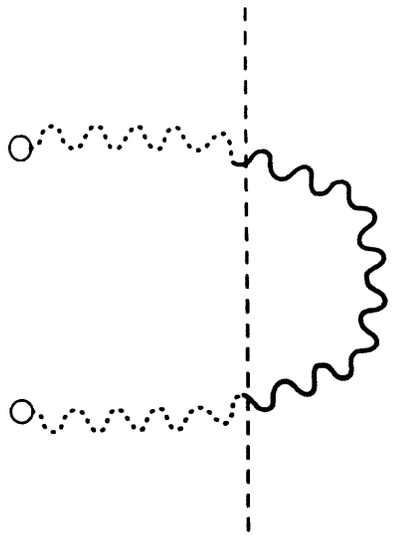

Fig. 12. The simplest R-term subgraph involving the gauge propagator. This too contributes to F_{hg} at the 6/3 order.

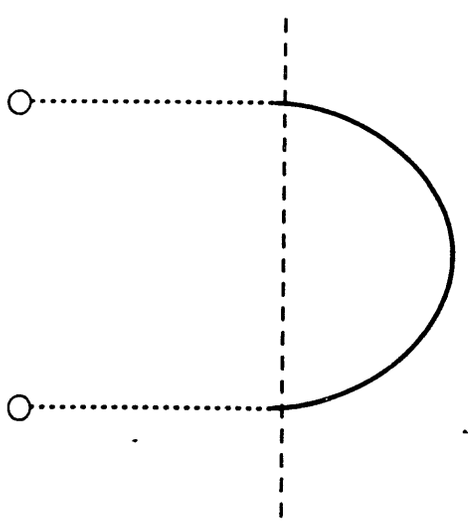

Fig. 13. Same as fig. 12 for the Higgs. This contributes to F_{hg} at the 8/3 order.

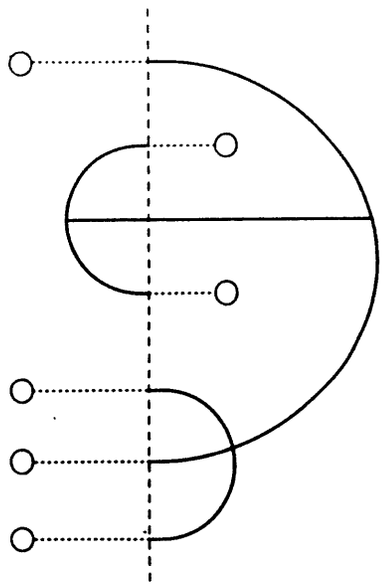

Fig. 14. A miscellaneous high-order contribution to F_{hg}.

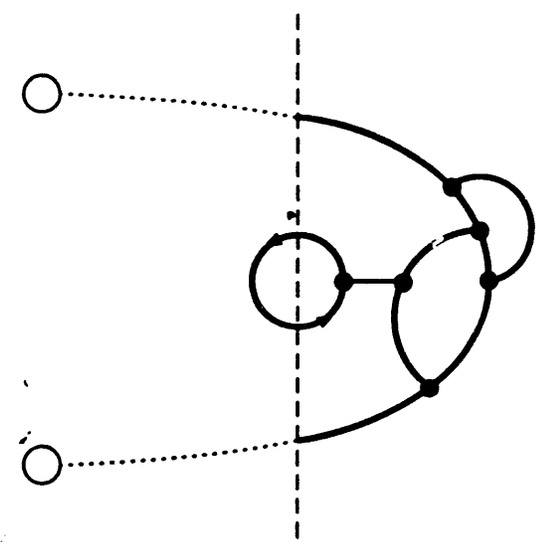

Fig. 15. An R-term diagram with loops. Such graphs do not contribute to F_{hg}. The directed line is a fermion loop, which corresponds to final-state fermion-antifermion pair production in the physical process. Thus fermion-antifermion production cannot contribute to F_{hg}.

in the Appendix of 't Hooft's paper,[12]

$$\bar{\eta}_{a\mu\nu}\bar{\eta}_{a\alpha\beta} \;=\; \delta_{\mu\alpha}\delta_{\nu\beta} - \delta_{\mu\beta}\delta_{\nu\alpha} - \epsilon_{\mu\nu\alpha\beta}\;, \tag{3.17}$$

after which the sum on polarizations is simple. The net result is that

$$\sum_{abc} \Pi_{ab}(\mathbf{k}) U'^{\dagger}_{bc} U_{ca} \to 3\omega_{\mathbf{k}}^2 + \mathbf{k}^2\;. \tag{3.18}$$

The integral in (3.15) is now straightforwardly performed, most conveniently in the relativistic limit $M_W^2(\Delta\xi)^2 \ll 1$, and gives for the contribution of fig. 10[35]

$$\frac{96\pi^2}{g^2}\frac{\rho^2\rho'^2}{\left((\Delta\xi_0+i\epsilon)^2-(\Delta\vec{\xi})^2\right)^2}. \tag{3.19}$$

The $i\epsilon$ here comes from the prescription $\Delta\xi_0 \to \Delta\xi_0 + i\epsilon$ needed to regulate the otherwise oscillatory and growing integrand.

We now wish to integrate over the remaining collective coordinates (ξ,ρ) and (ξ',ρ') in steepest descent approximation. To this order in the diagrammatic expansion, the exponent we are extremizing consists of three pieces. First there is fig. 10, given by Eq. (3.19). Second, there is the difference $iS[\phi]-iS[\phi']$ from Eq. (3.9), where ϕ and ϕ' are replaced by their classical instanton contributions, continued to Minkowski space. Of course, the *Minkowski* action of the *Minkowski* instanton just equals the *Euclidean* action of the ordinary *Euclidean* instanton, times a factor of $\pm i$ due to the change in integration measure $dx_0 \to \pm i dx_0$ (remember that ϕ and ϕ' are continued in the opposite directions). So this difference is just $-4\pi/\alpha_w - \pi^2(\rho^2+\rho'^2)v^2$ using Eq. (2.9). Third, there is a contribution of $-i(p_1+p_2)\cdot\Delta\xi$ coming from the initial-state phase factors $e^{-ip_1\cdot\Delta\xi}e^{-ip_2\cdot\Delta\xi}$ carried by the product $R^*(p_1)R^*(p_2)$ in Eq. (3.9). This factor is very important, as it is the only place where the energy of the incoming particles feeds into the calculation.

In the center-of-mass frame $p_1+p_2=(E,\mathbf{0})$ one therefore seeks to estimate the integral*

$$\int d^4(\Delta\xi)\int d\rho\int d\rho'\,\exp\Big\{-iE\Delta\xi_0 - \frac{4\pi}{\alpha_w} - \pi^2(\rho^2+\rho'^2)v^2 + \frac{96\pi^2}{g^2}\frac{\rho^2\rho'^2}{\left((\Delta\xi_0+i\epsilon)^2-(\Delta\vec{\xi})^2\right)^2}\Big\} \tag{3.20}$$

by saddle-point methods. A little algebra gives[35]

$$\Delta\vec{\xi}^{\,\text{saddle}} = 0, \quad \Delta\xi_0^{\text{saddle}} = i\left(\frac{24E}{\pi^2 g^2 v^4}\right)^{1/3}, \qquad \rho^{\text{saddle}} = \rho'^{\text{saddle}} = \left(\frac{3E^4}{8\pi^8 g^2 v^{10}}\right)^{1/6} \tag{3.21}$$

and hence[31,35,43]

$$\sigma_{\not B} \;\sim\; \exp\Big\{\frac{4\pi}{\alpha_w}\Big[-1+\frac{9}{8}\Big(\frac{E}{E_0}\Big)^{4/3}\Big]\Big\}, \quad E_0 = \sqrt{6}\pi\frac{M_W}{\alpha_w} \approx 20\,\text{TeV}\;, \tag{3.22}$$

confirming the back-of-the-envelope estimate (2.19) and, moreover, giving the constant with relative ease.

The threefold power of the R-term method is now apparent. First of all, we only needed to evaluate a *single* phase-space integral and polarization sum, Eqs. (3.15)-(3.16). In contrast, had we needed to confront n-particle phase space explicitly, Eq. (2.13), we would have struggled with the dizzying problem of constructing invariants from order $1/\alpha_w$ polarization and $\bar{\eta}$ tensors. Second, the quantity we are calculating, a generalized effective 'action', already lives in the exponent, so that we avoid the problem plaguing naive perturbation theory (Sec. 3.1), the out-of-control growth of diagrams with more and more disconnected components. Third, by examining at higher-order diagrams such

* Only the relative position coordinate $\Delta\xi$ enters in; the orthogonal combination gives an overall factor of the volume of space-time which is canceled by the initial-state flux factors.

as figs. 11-14, we find that their contributions to the holy grail function are suppressed by increasing powers of

$$\frac{\rho^2}{(\Delta\xi_0)^2} \sim \left(\frac{E}{E_{\rm sphal}}\right)^{2/3} \tag{3.23}$$

using Eq. (3.21). So when the sphaleron energy is approached from below, there is a *bona fide* perturbative treatment of the problem, the "small parameter" being $(E/E_{\rm sphal})^{2/3}$. The subleading $(E/E_0)^{6/3}$ contribution to F_{hg} has also been evaluated using R-term methods[44-46] and has a coefficient of $-9/16$, damping the growth in $\sigma_{\not B}$ implied by (3.22).† The new graphs that contribute at this order are fig. 11 (cf. Eq. (2.16)) and fig. 12. A partial calculation of the $(E/E_0)^{8/3}$ contribution can be found in Ref. [47].

Thus far, we have restricted our attention to tree graphs. That is because R-term diagrams with loops in them, such as fig. 15, do not contribute to F_{hg} at all. It is now clear why fermion-antifermion pair creation is unimportant, as mentioned earlier; when portrayed as R-term diagrams, such processes necessarily contain loops.

3.4. New improved instantons

If one seeks reliable answers when $E \sim E_{\rm sphal}$, the ratio $(E/E_{\rm sphal})^{2/3}$ is no longer small, and one needs to be able to sum the R-term tree graphs such as figs. 10-14 *all at once*. That means abandoning perturbation theory, and looking for solutions to the full classical Euler-Lagrange equations for ϕ and ϕ' (which once again stand for both Higgs and gauge fields) implied by the exponent of Eq. (3.9), including the R-term. Solutions of this equation are called 'new improved instantons' and are discussed in Ref. [25].

Let us split up ϕ and ϕ' into classical and fluctuating pieces as in Eq. (3.14), and focus on the coupled Euler-Lagrange equations for $\delta\phi$ and $\delta\phi'$. Furthermore, to get a feel for what the new improved instantons look like, let us discard

† The first calculation of this coefficient was actually performed using the valley method.[26]

all terms cubic and quartic in $\delta\phi$ and $\delta\phi'$ coming from the classical actions in Eq. (3.9); this is valid at low energies. The resulting equations will then be linear, since the R-term is at most bilinear in $\delta\phi$ and $\delta\phi'$. Specifically, they have the following form:

$$\begin{pmatrix} D & -\hat{\mathsf{R}} \\ -\hat{\mathsf{R}}^* & D' \end{pmatrix} \begin{pmatrix} \delta\phi \\ \delta\phi' \end{pmatrix} = \begin{pmatrix} \hat{\mathsf{R}} & 0 \\ 0 & \hat{\mathsf{R}}^* \end{pmatrix} \begin{pmatrix} \phi'_{\rm inst} \\ \phi_{\rm inst} \end{pmatrix} + \mathcal{O}(\delta\phi^2, \delta\phi'^2) \,. \tag{3.24}$$

Here D (D') represents the second-order differential operator for the fluctuating field in the background of an instanton of size ρ (ρ') centered at ξ (ξ'); $\hat{\mathsf{R}}$ is the kernel of the R-term, Eq. (3.10). In order to solve these equations, one needs to be able to invert the operators D and D'. But these inverses are by definition, the Levine-Yaffe propagators G and G' in the instanton background[37,38] (see Sec. 5.1 below).

Eq. (3.24) implies the following linearized approximation to the new improved instantons $\phi_{\rm new}$ and $\phi'_{\rm new}$:

$$\begin{aligned} \phi_{\rm new} &\equiv \phi_{\rm inst} + \delta\phi \simeq \phi_{\rm inst} + G\hat{\mathsf{R}}^*\phi'^*_{\rm inst} + G\hat{\mathsf{R}}^*G'\hat{\mathsf{R}}\phi_{\rm inst} + \cdots \,, \\ \phi'_{\rm new} &\equiv \phi'_{\rm inst} + \delta\phi' \simeq \phi'_{\rm inst} + G'\hat{\mathsf{R}}^*\phi^*_{\rm inst} + G'\hat{\mathsf{R}}^*G\hat{\mathsf{R}}\phi'_{\rm inst} + \cdots \,. \end{aligned} \tag{3.25}$$

Index contraction and momentum integration is understood in the compact notation of Eq. (3.25).

Closed-form expressions for linearized new improved instantons can be found in Ref. [25], but we can already make an observation just from looking at Eq. (3.25). The fact that $\phi_{\rm new}$ depends on $\phi'_{\rm inst}$ and that $\phi'_{\rm new}$ depends on $\phi_{\rm inst}$ means that $\phi_{\rm new}$ and $\phi'_{\rm new}$ cannot be $O(4)$ symmetric as are the ordinary zero-energy instantons $\phi_{\rm inst}$ and $\phi'_{\rm inst}$. The reason is that the axis separating their centers is a distinguished direction in space. The remaining symmetry is a cylindrical symmetry about this axis, namely $O(3)$.

As the R-term is only defined in Minkowski space, the instantons and propagators that appear in Eq. (3.25) must all be understood in their Minkowski continuation. In fact, it appears impossible to continue new improved instantons to Euclidean space. The reason is that they contain $i\epsilon$ prescriptions such as

the one in Eq. (3.19) which impede the Wick rotation.* This fact makes new improved instantons awkward for purposes of numerical calculation. Fortunately, there is another, seemingly orthogonal approach to distorted instantons, the valley method, that lives happily in Euclidean space, and which we now review.

3.5. The valley approach of Khoze, Ringwald, Balitsky and Yung

In ordinary perturbation theory, a total $2 \to$ any cross section is most conveniently calculated indirectly, via the optical theorem, as the imaginary part of a forward $2 \to 2$ amplitude. That this idea could be usefully applied to total *anomalous* cross sections was first suggested by Zakharov[31] and Porrati,[43] who extracted the leading-order $(E/E_{sphal})^{4/3}$ contribution to F_{hg} by isolating the contributions to the forward amplitude due to far-separated instanton-antiinstanton ($I\bar{I}$) pairs (see fig. 16). Here "far separated" means

$$\frac{\rho^2}{R^2} \ll 1 , \tag{3.26}$$

where ρ is the typical size of the instanton or antiinstanton and R is the $I\bar{I}$ separation. Experience with the R-term approach suggests that this condition is valid only at low energies, $E \ll E_{sphal}$ (see Eq. (3.23)). At higher energies the instanton and antiinstanton begin to overlap, and their interaction causes them to distort. One needs a more powerful formalism to describe this physics.

Such an approach to calculating the anomalous cross section is the *valley method* employed by Khoze and Ringwald,[26,27,48,49] based on work by Balitsky and Yung.[50,51] The basic observation[50,51] is that a far-separated and undistorted $I\bar{I}$ pair can be viewed as an endpoint of a finite-parameter family of configurations known as the valley, along which the Euclidean action is slowly varying. In the limit $g^2 \to 0$, the orthogonal directions in function space, the "canyon walls" surrounding the valley, become very steep, and can be treated in Gaussian approximation. In fact, for purposes of calculating the holy grail function, these Gaussian integrations can be completely neglected, as they only

* Field theorists will recognize this type of $i\epsilon$ prescription as characteristic of Wightman functions rather than Feynman propagators.

give a preexponential contribution to the cross section. All that one really needs to know is the action along the valley.

To be more specific, in a generic theory, let $\phi_1(x;\xi_1,\rho_1)$ and $\phi_2(x;\xi_2,\rho_2)$ denote an instanton and antiinstanton, respectively, centered at $\xi_{1,2}$ and with scale size $\rho_{1,2}$. In the large-separation limit (3.26), the joint configuration

$$\phi_1(x;\xi_1,\rho_1) + \phi_2(x;\xi_2,\rho_2) \tag{3.27}$$

becomes an exact solution of the classical Euclidean equations of motion. What symmetries does this limiting solution possess? Aside from the exact translational zero modes generated by $\delta\xi_1^\mu = \delta\xi_2^\mu = \epsilon^\mu$, there are *quasi*zero modes $\delta\xi_1^\mu = -\delta\xi_2^\mu = \epsilon^\mu$. Furthermore, if the theory is (approximately) conformally invariant, there are also quasizero modes of the form $\rho_{1,2} \to \rho_{1,2} + \delta\rho_{1,2}$. As the $I\bar{I}$ configuration flows along these *almost* flat directions, the instanton and antiinstanton begin to deform. These distorted instantons are quite similar to the new improved instantons of Sec. 3.4, in that the full spherical symmetry breaks down to a cylindrical $O(3)$ symmetry along the $I\bar{I}$ axis. The compelling advantage of the valley method is that these distorted configurations are defined from the start in Euclidean space, so that the necessary numerical computations are much more straightforward.

Let $\Phi_\tau(x)$ denote the valley configuration parametrized by the finite number of collective coordinates τ_i of the $I\bar{I}$ system. What equation does Φ_τ satisfy? Only for $R \to \infty$ will Φ_τ be a solution of the classical equations of motion. In that limit, as we saw, Φ_τ approaches the sum (3.27). For finite R, Φ_τ will *still* solve the classical equation—provided the variations are constrained to be orthogonal to the (quasi)zero modes of the valley. That is,

$$\left\langle (\phi - \Phi_\tau), \frac{\partial \Phi_\tau}{\partial \tau_i} \right\rangle_w = 0 , \tag{3.28}$$

where $\langle\ ,\ \rangle_w$ denotes the functional inner product

$$\langle A, B \rangle_w = \int dx\, A(x)\, w(x;\tau)\, B(x) \tag{3.29}$$

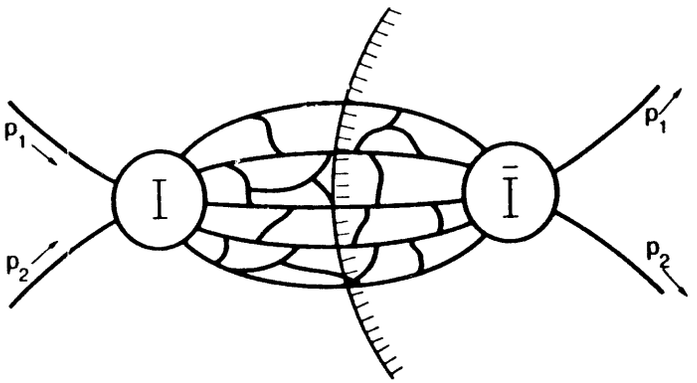

Fig. 16. The total anomalous cross section as the imaginary part of a nonanomalous forward amplitude with an instanton-antiinstanton pair in the intermediate state.

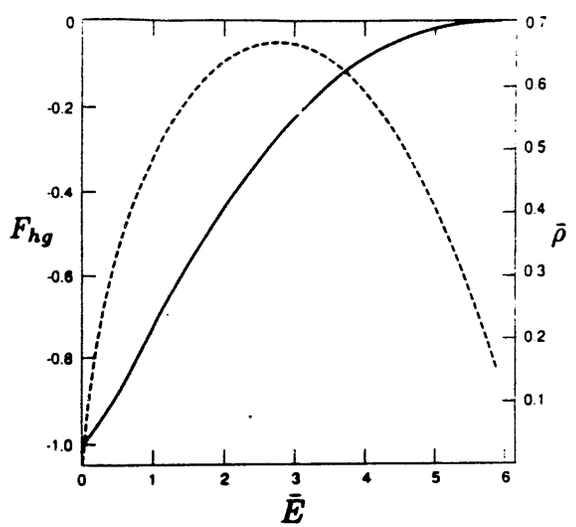

Fig. 17. The holy grail function F_{hg} (solid line, left axis) as a function of rescaled center-of-mass energy $\bar{E} = \alpha_w E/\pi M_W \approx E/(8\,\mathrm{TeV})$, in the approximate model of Khoze and Ringwald. Thus in this model, B violation is no longer exponentially suppressed when $E \approx 40\,\mathrm{TeV}$. Also shown is the rescaled instanton size $\bar{\rho} = \rho M_W$ (dotted line, right axis), which mysteriously decreases starting at $\approx 20\,\mathrm{TeV}$. This figure is taken from Ref. 27.

and w is some positive-definite weight function. Formally, these constraints are implemented by inserting a Fadeev-Popov factor of unity

$$1 = \int \prod_i d\tau_i \, J_\tau \prod_j \delta\big(\langle(\phi - \Phi_\tau), \tfrac{\partial \Phi_\tau}{\partial \tau_j}\rangle_w\big) \tag{3.30}$$

into the path integral. J_τ denotes the Jacobean $J_\tau = |\det J_{mn}|$ associated with the constraints, where

$$J_{mn} = \left\langle (\phi - \Phi_\tau), \frac{\partial^2 \Phi_\tau}{\partial \tau_m \partial \tau_n} \right\rangle_w - \left\langle \frac{\partial \Phi_\tau}{\partial \tau_m}, \frac{\partial \Phi_\tau}{\partial \tau_n} \right\rangle_w . \tag{3.31}$$

Exponentiating these δ-functions by means of the identity

$$\delta(a) = \frac{1}{2\pi} \int d\lambda \, e^{i\lambda a} , \tag{3.32}$$

one immediately arrives at the desired "valley equation,"[50,51]

$$\left.\frac{\delta S_E}{\delta \phi}\right|_{\phi = \Phi_\tau} = i \sum_j \lambda_j(\tau)\, w(x;\tau) \frac{\partial \Phi_\tau}{\partial \tau_j} . \tag{3.33}$$

The $i\lambda_j$ play the role of Lagrange multipliers. In principle, Eq. (3.33) can be solved numerically for Φ_τ and $i\lambda_j$, starting with the large-separation boundary conditions (3.27) and gradually reducing R. Despite appearances, the $i\lambda_j$ will stationarize at *real* values.

A simple example of this program is double-well quantum mechanics, examined by Balitsky and Yung.[50] In this case,

$$S_E[\phi] = \int dt \big(\tfrac{1}{2}(\partial_t \phi)^2 + \alpha(\phi^2 - v^2)^2\big) \tag{3.34}$$

where t is Euclidean time, and the approximate $I\bar{I}$ solution, valid for large R, is the sum of the familiar kink and antikink,

$$\Phi_{\{\xi,R\}} \doteq v\Big\{ \tanh \tfrac{1}{2} m(t - \xi + R/2) - \tanh \tfrac{1}{2} m(t - \xi - R/2) - 1 \Big\} \tag{3.35}$$

with $m = v\sqrt{8\alpha}$. Unity has been subtracted in (3.35) in order to satisfy the vacuum condition $\Phi \to -v$ as $t \to \pm\infty$. The valley equation

$$-\partial_t^2 \Phi + 4\alpha\Phi(\Phi^2 - v^2) = i\lambda_R \partial_R \Phi + i\lambda_\xi \partial_\xi \Phi \tag{3.36}$$

subject to the boundary condition (3.35) can be solved in a small-fluctuations expansion:

$$\Phi_{\{\xi,R\}} \;=\; v\Big\{a\tanh\tfrac{1}{2}M(t-\xi+R/2)-a\tanh\tfrac{1}{2}M(t-\xi-R/2)-1\Big\} \quad (3.37)$$

and

$$i\lambda_\xi \;=\; 0, \qquad i\lambda_R \;=\; 6m^2\epsilon^2+\mathcal{O}(\epsilon^4) \quad (3.38)$$

where

$$a=1-\tfrac{3}{2}\epsilon^2+\mathcal{O}(\epsilon^4), \quad M=m(1-\tfrac{3}{2}\epsilon^2+\mathcal{O}(\epsilon^4)), \quad \text{and } \epsilon=\operatorname{sech}(MR/2). \quad (3.39)$$

The fact that the Lagrange multiplier λ_ξ associated with the exact translational zero mode vanishes follows immediately from Eq. (3.36) if one multiplies both sides by $\partial_\xi\Phi\equiv-\partial_t\Phi$ and integrates over t.

In Eq. (3.36), the simplest choice of weight function has been made, $w=1$. In general, different choices of weight functions w lead to different valleys. Given this inherent ambiguity, what constitutes a 'good' choice of w? A technical condition has been formulated by Yung,[51] but loosely speaking, a good choice of w is one in which the right-hand side of the valley equation (3.33) is perturbatively small once the λ_i have been solved for. If that is the case, then the valley truly can be spanned by approximate zero modes.

Interestingly, it is possible to choose w so that the undistorted kink-antikink sum, Eq. (3.35), remains an exact solution of the valley equation even for small R.[48,52] This choice makes clear a general feature of the valley configurations:[51] as Eq. (3.35) suggests, they interpolate smoothly between a well-separated $I\bar{I}$ pair at one extreme, and the ordinary perturbative vacuum at the other extreme, as R decreases from infinity to zero.

Of course, what we are really interested in is 4-dimensional gauge theories, not 1-dimensional quantum mechanics. In Electroweak theory, as of this writing, the solution of the coupled valley equations for the gauge and Higgs sectors is not known, not even numerically. But in QCD, it is. The reason stems from a remarkable sequence of manipulations discussed by Yung.[51] Start with a widely separated $I\bar{I}$ pair, and use the conformal transformation properties of QCD[53]

to map this configuration onto one in which the instanton and antiinstanton are concentric about the origin. Doing so requires that we first translate I and $\bar{I}$ so that their centers $\xi_{1,2}$ are collinear and satisfy $\xi_1^\mu(\xi_2^2+\rho_2^2)=\xi_2^\mu(\xi_1^2+\rho_1^2)$, and then apply the inversion-dilatation transformation

$$x_\lambda \;\to\; \frac{x_\lambda r^2}{x^2}, \qquad A_\mu^a(x_\lambda) \;\to\; \frac{r^2}{x^2}\Big(\delta_{\mu\alpha}-\frac{2x_\mu x_\alpha}{x^2}\Big)A_\alpha^a(x_\lambda r^2/x^2) \quad (3.40)$$

with arbitrary r^2, followed by a translation to the origin. The invariant quantity in all of this is the dimensionless combination of $I\bar{I}$ parameters*

$$\tilde{z} \;=\; \frac{R^2+\rho_1^2+\rho_2^2}{2\rho_1\rho_2}, \quad 1\le\tilde{z}<\infty\,. \quad (3.41)$$

Since the initial widely separated configuration had $\tilde{z}\simeq R^2/2\rho_1\rho_2\gg1$, the final concentric configuration, with $R=0$, must have either $\rho_1\gg\rho_2$ or $\rho_2\gg\rho_1$.

Yung's next step is to focus on the subset of configurations centered at the origin with the following tensor structure:

$$A_\mu^a(x) \;=\; \frac{2}{g}\frac{\bar{\eta}_{a\mu\nu}x_\nu}{x^2}\phi(x^2)\,. \quad (3.42)$$

Note that this restricted subset is nonetheless broad enough to encompass *both* instantons and antiinstantons:

$$\begin{aligned}\phi(x^2) &= \frac{\rho^2}{x^2+\rho^2} \;\longleftrightarrow\; \text{instanton in singular gauge}\\ \phi(x^2) &= \frac{x^2}{x^2+\rho^2} \;\longleftrightarrow\; \text{antiinstanton in regular gauge}\,.\end{aligned} \quad (3.43)$$

Surprisingly, when restricted to the configurations (3.42), the Euclidean action of QCD becomes just that of the (rescaled) quantum-mechanical double well:

$$S_E[\phi] \;=\; \frac{48\pi^2}{g^2}\int dt\,\big(\tfrac{1}{2}(\partial_t\phi)^2+\tfrac{1}{2}\big[(\phi-\tfrac{1}{2})^2-\tfrac{1}{4}\big]^2\big)\,, \quad t=\log x^2\,. \quad (3.44)$$

* Under inversions $\xi_i^\mu\to r^2\xi_i^\mu/(\xi_i^2+\rho_i^2)$ and $\rho_i\to r^2\rho_i/(\xi_i^2+\rho_i^2)$ so that $\tilde{z}\to\tilde{z}$; translation and dilatation invariance of $\tilde{z}$ is obvious.

Furthermore, with the substitution $t = \log x^2$, the (anti)kinks $\frac{1}{2}(1 \mp \tanh \frac{1}{2}(t - t_0))$ map precisely into the (anti)instantons (3.43) with $\rho^2 = e^{t_0}$. Thus a far-separated kink-antikink pair corresponds to a concentric $I\bar{I}$ pair with $\rho_1 \ll \rho_2$ or $\rho_2 \ll \rho_1$, which, in turn, is conformally equivalent to a far-separated $I\bar{I}$ pair as we saw.

This last observation suggests the third and final step, which is to identify the full $I\bar{I}$ valley in QCD with those configurations that map onto the valley in the double well problem discussed previously (likewise for the weight functions). This choice does not guarantee that the QCD valley equation is satisfied, but indeed it is, due to the fact that Yung's ansatz (3.42) corresponds to $I\bar{I}$ pairs with the maximally attractive relative orientation.[51] If one follows through with this procedure, one finds that the ***undistorted*** kink-plus-antikink valley (3.35) corresponds to a *distorted* $I\bar{I}$ pair in QCD whose action is[27,52]

$$S_{\rm val}(z) = \frac{48\pi^2}{g^2}\left[\frac{6z^2-14}{(z-1/z)^2} - \frac{17}{3} - \log z\Big(\frac{(z-5/z)(z+1/z)^2}{(z-1/z)^3} - 1\Big)\right], \qquad z = \tilde{z} + \sqrt{\tilde{z}^2 - 1}\,. \tag{3.45}$$

The great simplification due to conformal invariance is evident in the fact that the action depends on the single variable $\tilde{z}$ defined in Eq. (3.41). As $\tilde{z}$ is lowered from ∞ to 1, $S_{\rm val}(z)$ drops monotonically from $2S_{cl} = 16\pi^2/g^2$ to 0, reflecting the gradual collapse of the $I\bar{I}$ configuration into the perturbative vacuum.

Based on these QCD expressions, a crude nonperturbative model of anomalous B violation in Electroweak theory can now be had, following Khoze and Ringwald, by taking[27]

$$\sigma_{\not B} \sim {\rm Im} \int dR\, d\rho_1\, d\rho_2\, \exp\left\{ER - \pi^2(\rho_1^2 + \rho_2^2)v^2 - S_{\rm val}(z)\right\}. \tag{3.46}$$

The first term in the exponent is the Euclidean equivalent of the initial-state phase factor $-iE\Delta\xi_0$ in Eq. (3.20). The second and third terms in the exponent represent the conformally invariant QCD valley action (3.45), augmented by the infrared cutoff from Eq. (2.9) characterizing Electroweak instantons. In all other respects the Higgs degrees of freedom are ignored in this model. Obviously the integral formally diverges as $R \to \infty$, but that is precisely the unstable mode necessary to give a factor of i and hence a nonzero, and finite, imaginary part in Gaussian approximation.

The numerical results of this calculation are displayed in fig. 17. Plotted is the holy grail function $\frac{\alpha_W}{4\pi}\log\sigma_{\not B}$ versus total center-of-mass energy E. We see that in this model, the B-violating cross section becomes observably large when $E \sim 40\,{\rm TeV}$. Furthermore, F_{hg} never crosses zero, so that there is no problem with the unitarity bound. One would expect the general features of this curve to survive a more ambitious calculation in which conformal invariance is abandoned, and the full coupled gauge and Higgs valley equations are solved. Bear in mind that ***only final-state corrections*** are taken into account in the valley method as used to date. As in the R-term approach, the initial-state quanta are simply modeled by the phase factor ER in the exponent of (3.46).

3.6. Equivalence of valley and R-term methods

When the valley method was first adapted to the calculation of the total B-violating cross section, it is fair to say that it was greeted with some skepticism. The reason is that there is no topological distinction between a distorted $I\bar{I}$ pair and a vacuum-sector configuration. Distinguishing these two types of intermediate states is crucial: the slightest admixture of a vacuum-sector excitation will swamp $\sigma_{\not B}$ with the much larger total *non*anomalous cross-section. This issue is especially troublesome when the instanton and antiinstanton sit nearly on top of one another, as they do in high energies in Weinberg-Salam theory. It was therefore surprising to workers in the field that in Weinberg-Salam theory, the valley and R-term methods precisely agree at least through the $(E/E_{\rm sphal})^{6/3}$ coefficient of the holy grail function F_{hg}.[26,35,44–46]

In fact, this agreement was no accident of low orders. We now sketch the main elements of a recent proof[36] that the valley and R-term methods are perturbatively equivalent to all orders in the expansion parameter $(E/E_{\rm sphal})^{2/3}$ (including logarithms). For purposes of the proof, it is convenient to expand,

not about the valley itself, but rather about the naive $I\bar{I}$ sum (3.27). That is, we let

$$\Phi(x) \;=\; \phi_1(x;\xi_1,\rho_1) + \phi_2(x;\xi_2,\rho_2) + \chi(x)\;, \tag{3.47}$$

where for the remainder of this Section ϕ_1 (ϕ_2) denotes the Minkowski-continued (anti)instanton, and we consider perturbation theory in the fluctuating field χ. Since we will work formally to all orders in χ, this procedure is equivalent to expanding about the solution to the valley equation (3.33). The proof that follows is model independent, but for simplicity we will focus on the theory of a real scalar field in D dimensions, with action

$$\begin{aligned} iS[\Phi] &= i\int \mathrm{d}^D x\,\left(\tfrac{1}{2}(\partial_\mu\Phi)^2 - \tfrac{1}{2}m^2\Phi^2 - V(\Phi)\right) \\ &= -2S_{cl} + i\int \mathrm{d}^D x\Big\{\tfrac{1}{2}(\partial_\mu\chi)^2 - \tfrac{1}{2}m^2\chi^2 + \chi\Big(\tfrac{\delta V(\phi_1)}{\delta\phi_1} + \tfrac{\delta V(\phi_2)}{\delta\phi_2}\Big) \\ &\quad + V(\phi_1) + V(\phi_2) - V(\phi_1+\phi_2+\chi) + \tfrac{1}{2}\phi_1\tfrac{\delta V(\phi_2)}{\delta\phi_2} + \tfrac{1}{2}\phi_2\tfrac{\delta V(\phi_1)}{\delta\phi_1}\Big\}\;. \end{aligned} \tag{3.48}$$

Here we have used the Minkowski-space (anti)instanton equation of motion,

$$\Box\phi_l + m^2\phi_l + \frac{\delta V(\phi_l)}{\delta\phi_l} = 0\;, \qquad l = 1,2\;, \tag{3.49}$$

to eliminate quadratic cross-terms such as $\phi_1(\Box + m^2)\phi_2$.

The strategy of the proof is to use Cutkosky's cutting rules[30] to relate the connected $2 \to 2$ diagrams generated by (3.48) to connected R-term diagrams of the sort discussed in Sec. 3.3. A technical point: it will be necessary to assume that in momentum space, the Euclidean (anti)instanton is a holomorphic function defined on the complex k^2 plane except for simple poles and cuts along the negative-k^2 axis. Cauchy's theorem then implies the existence of a spectral representation, which follows from wrapping the contour around the negative axis. For instantons in Minkowski space, the spectral representation reads:

$$\phi_l(k) = \int_0^\infty \mathrm{d}(\mu^2)\sigma_l(\mu^2)\frac{i}{k^2-\mu^2+i\epsilon}\;, \quad l = 1,2\;. \tag{3.50}$$

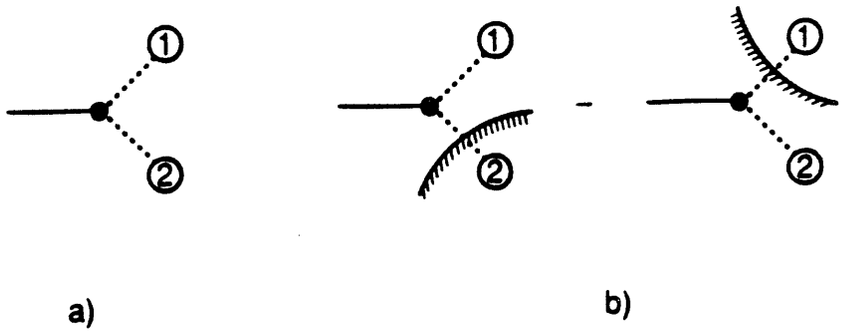

Fig. 18. (a) The $-ig\chi\phi_1\phi_2$ vertex. (b) The two possible vertices after cutting, representing $-ig\chi_1\phi_1\phi_2^- + ig\chi_2\phi_1^+\phi_2^*$.

A specific example to keep in mind is the QCD instanton in singular gauge,[15,12] which can be written as[39]

$$\begin{aligned} A^{\mu a}_{\rm inst}(k) &\equiv \frac{2\rho^2}{g}U_{ab}\int d^4x\, e^{ik\cdot(x-\xi)}\,\frac{\bar\eta_{b\mu\nu}(x_\nu-\xi_\nu)}{\left[(x-\xi)^2-i\epsilon\right]\left[(x-\xi)^2-\rho^2-i\epsilon\right]} \\ &= -\frac{4\pi^2\rho^2}{g}U_{ab}\,\bar\eta_{b\mu\lambda}\,k_\lambda\int_0^\infty \mathrm{d}(\mu^2)\,\sigma(\mu^2)\frac{i}{k^2-\mu^2+i\epsilon} \end{aligned} \tag{3.51}$$

where

$$\sigma(\mu^2) \;=\; \delta(\mu^2) + \frac{\rho}{4\mu}\big(J_1(\mu\rho) + J_3(\mu\rho)\big)\;. \tag{3.52}$$

The δ-function reflects the isolated mass-shell pole exploited by Ringwald and Espinosa, while the Bessel functions represent the two- and higher-particle cuts, which are generated by iteration of Eq. (3.49).

Eq. (3.50) makes manifest the essential similarity between the Minkowski-continued (anti)instanton $\phi_l(x;\xi)$ and a generic Feynman propagator $G_F(x,\xi)$

in its Lehmann representation. In particular, just like a Feynman propagator, ϕ_l can be decomposed into positive and negative frequency modes ("Wightman functions"):

$$\phi_l(x;\xi) = \theta(x_0-\xi_0)\phi_l^+(x;\xi) + \theta(\xi_0-x_0)\phi_l^-(x;\xi) \tag{3.53}$$

with

$$\phi_l^\pm(x;\xi) = \phi_l^\mp(\xi;x) = \int \frac{\mathrm{d}^D k}{(2\pi)^{D-1}} e^{-ik\cdot(x-\xi)}\theta(\pm k_0)\int_0^\infty \mathrm{d}(\mu^2)\sigma_l(\mu^2)\delta(k^2-\mu^2)\,. \tag{3.54}$$

Unlike for true propagators, the spectral functions σ_l are not necessarily positive real functions, but that is irrelevant for purposes of the cutting rules.

It is desirable to have a systematic method for applying the cutting rules to the various interaction terms in (3.48). *We will do so by modifying the Lagrangian directly.* As an illustration of this technique, consider the possible cubic vertex $-ig\chi\phi_1\phi_2$ arising from the expansion of $-iV(\phi_1+\phi_2+\chi)$. This vertex is pictured in fig. 18a. Upon application of the cutting rules, it should be replaced by the sum of two vertices, $-ig\chi_1\phi_1\phi_2^- + ig\chi_2\phi_1^+\phi_2^*$, which account for the cut running either above or below the vertex, as in fig. 18b. Here χ_1 and χ_2 denote the two distinct fluctuation fields induced, depending on which side of the cut they lie on. In this manner, the full set of interaction terms in Eq. (3.48) is doubled in length to read

$$\begin{aligned} i\int \mathrm{d}^D x\Big\{ &\chi_1\Big(\tfrac{\delta V(\phi_1)}{\delta\phi_1} + \tfrac{\delta V(\phi_2^-)}{\delta\phi_2^-}\Big) - \chi_2\Big(\tfrac{\delta V(\phi_1^+)}{\delta\phi_1^+} + \tfrac{\delta V(\phi_2^*)}{\delta\phi_2^*}\Big) + V(\phi_1) - V(\phi_1^+) \\ &- V(\phi_2^*) + V(\phi_2^-) - V(\phi_1+\phi_2^-+\chi_1) + V(\phi_1^+ + \phi_2^* + \chi_2) \\ &+ \tfrac{1}{2}\phi_1\tfrac{\delta V(\phi_2^-)}{\delta\phi_2^-} - \tfrac{1}{2}\phi_1^+\tfrac{\delta V(\phi_2^*)}{\delta\phi_2^*} + \tfrac{1}{2}\phi_2^-\tfrac{\delta V(\phi_1)}{\delta\phi_1} - \tfrac{1}{2}\phi_2^*\tfrac{\delta V(\phi_1^+)}{\delta\phi_1^+}\Big\}\,. \end{aligned} \tag{3.55}$$

The requisite propagators for χ_1 and χ_2 are generated by the action

$$i\int \mathrm{d}^D x\{\tfrac{1}{2}(\partial_\mu\chi_1)^2 - \tfrac{1}{2}m^2\chi_1^2 - \tfrac{1}{2}(\partial_\mu\chi_2)^2 + \tfrac{1}{2}m^2\chi_2^2\} + \chi_2\hat{\mathrm{R}}\chi_1\,, \tag{3.56}$$

where $\hat{\mathrm{R}}$ is the R-term operator defined in Eq. (3.10). This quadratic form is straightforwardly inverted to give what the cutting rules dictate (see Eq. (3.13) *ff.*).

In summary, we have constructed a new "action" iS_{cut}, defined by the sum of (3.55) and (3.56). iS_{cut} serves as a concise bookkeeping device for generating automatically all possible cuttings of Eq. (3.48) with the correct combinatorics. The path integration now runs over the two independent fields χ_1 and χ_2 instead of just χ.

To attain our goal, we need the equations of motion for $\phi_l^\pm$, which are derived as follows. Fig. 19a illustrates the defining equation for the instanton, Eq. (3.49), for the particular choice of potential $V = \frac{g}{3}\phi^3 + \frac{\lambda}{4}\phi^4$. Taking the discontinuity of this equation leads to fig. 19b. Iterating fig. 19a to eliminate the last two graphs of fig. 19b leads finally to fig. 19c, which is equivalent, for general V, to the statements

$$\Box\phi_1^+ + m^2\phi_1^+ + \frac{\delta V(\phi_1^+)}{\delta\phi_1^+} - i\hat{\mathrm{R}}\phi_1 = 0 \tag{3.57}$$

and likewise

$$\Box\phi_2^- + m^2\phi_2^- + \frac{\delta V(\phi_2^-)}{\delta\phi_2^-} + i\hat{\mathrm{R}}^*\phi_2^* = 0\,. \tag{3.58}$$

With the help of Eqs. (3.49), (3.57) and (3.58), and some integrations by parts, one can rewrite iS_{cut} in the following suggestive form:

$$\begin{aligned} iS_{\mathrm{cut}} = i\int d^D x\Big\{&\tfrac{1}{2}\big(\partial_\mu(\chi_1+\phi_2^-)\big)^2 - \tfrac{1}{2}m^2(\chi_1+\phi_2^-)^2 \\ &- V(\phi_1+\chi_1+\phi_2^-) + V(\phi_1) + (\chi_1+\phi_2^-)V'(\phi_1)\Big\} \\ -i\int d^D x\Big\{&\tfrac{1}{2}\big(\partial_\mu(\chi_2+\phi_1^+)\big)^2 - \tfrac{1}{2}m^2(\chi_2+\phi_1^+)^2 \\ &- V(\phi_2^*+\chi_2+\phi_1^+) + V(\phi_2^*) + (\chi_2+\phi_1^+)V'(\phi_2^*)\Big\} \\ &+ (\phi_2^*+\chi_2)\hat{\mathrm{R}}(\phi_1+\chi_1) + iS[\phi_1^+] - iS[\phi_2^-]\,. \end{aligned} \tag{3.59}$$

$S[\phi_l^\pm]$ is the quantity obtained by stuffing $\phi_l^\pm$ into the classical action. Actually it is easy to see that

$$S[\phi_1^+] = S[\phi_2^-] = 0\,; \tag{3.60}$$

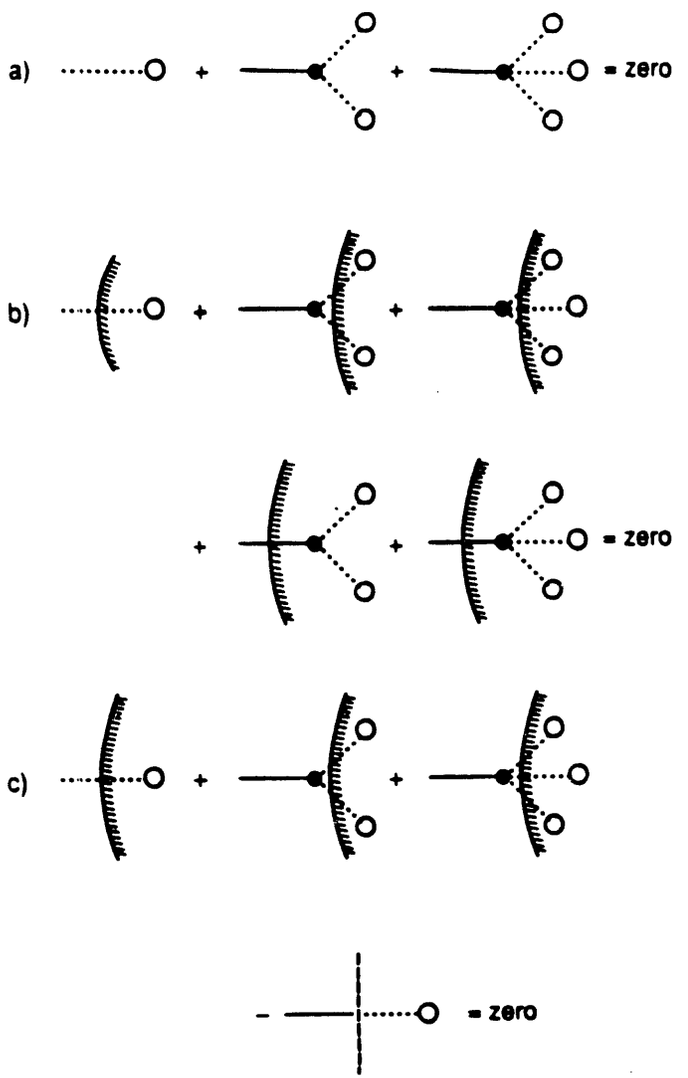

. 19. (a) The equation of motion (3.49) for the instanton ϕ_1. The potential has been chosen to be $\frac{g}{3}\phi^3 + \frac{\lambda}{4}\phi^4$. (b) The discontinuity of the instanton equation of motion. (c) The equation of motion (3.57) for the instanton's Wightman function ϕ_1^+. Instanton lines cut by hashmarks are ϕ_1^+. The straight dashed line is the $\hat{R}$ operator, Eq. (3.10), which results from cutting a free propagator (solid line).

simply write out the various integrals in momentum space, and observe that expressions like $\delta^D(p+q+k)\theta(p_0)\theta(q_0)\theta(k_0)$ vanish. The formal equivalence between the valley and R-term methods is now readily established by performing the shift of path integration variables

$$\chi_1 \to \chi_1 - \phi_2^- , \qquad \chi_2 \to \chi_2 - \phi_1^+ \tag{3.61}$$

in Eq. (3.59), and noting that

$$\hat{R}\phi_2^- = \phi_1^+\hat{R} = 0 \tag{3.62}$$

since $\theta(k_0)\theta(-k_0) = 0$. *QED*

4. Multi-Instanton Corrections

4.1. The Zakharov-Maggiore-Shifman model for the breakdown of the dilute instanton gas approximation

Thus far in these Lectures, we have restricted our instanton calculations to the *dilute gas* approximation. That is, we have expanded about the naive Ringwald-Espinosa substitution

$$\phi(x) \longrightarrow \phi_{\rm inst}(x;\xi,\rho) \tag{4.1}$$

instead of, say,

$$\phi(x) \longrightarrow \phi_{\rm inst}(x;\xi_1,\rho_1) + \phi_{\rm inst}(x;\xi_2,\rho_2) + \bar{\phi}_{\rm inst}(x;\xi_3,\rho_3) \tag{4.2}$$

where the right-hand side consists of two instantons plus one antiinstanton and so still changes $N_{\rm CS}$ by one unit. Indeed, most of the workers in B violation who have speculated on the role of multiinstanton configurations such as (4.2) have assumed that these cannot be significant until such energies that single-instanton amplitudes themselves have gotten observably large (if that ever happens), at which energies the multiinstantons help to unitarize $\sigma_{\not B}$.[22,54] This intuition is ingrained from quantum mechanical examples such as the double

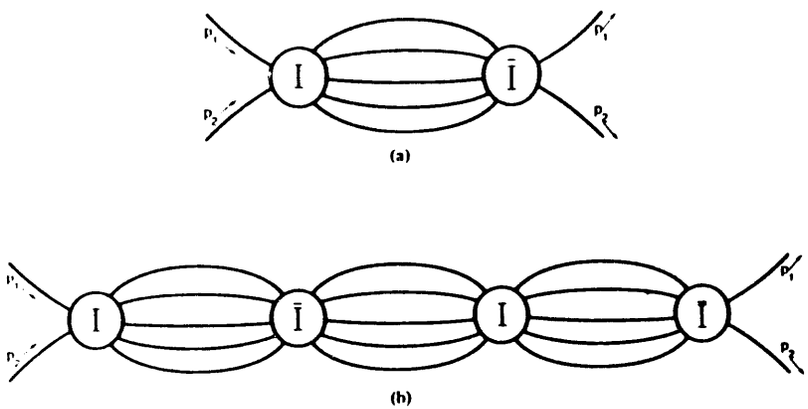

Fig. 20. The first two in an infinite series of contributions to the forward amplitude with more and more instanton-antiinstanton pairs arranged in a chain.

well, where back-and-forth transitions between the two wells can be neglected until the energy reaches the potential barrier E_{sphal}, which is precisely the point where the one-instanton tunneling amplitude loses its exponential suppression. If this is also the case in field theory, then multiinstantons can be safely ignored for purposes of answering the fundamental question, Does $\sigma_{\not B}$ become observably large at accelerator energies?

In light of this intuition come the surprising claims by Zakharov[5,55] and Maggiore and Shifman[56] that multiinstanton effects become important *long before* the one-instanton amplitude has grown large. The basic argument is easily summarized. These authors use an effective Lagrangian approach (more on this below) in which (anti)instanton interactions are represented by effective nonrenormalizable multiparticle vertices.[57] In this language, a forward $2 \to 2$ amplitude is represented by a sequence of diagrams as shown in fig. 20; $\sigma_{\not B}$ is then extracted via the optical theorem through appropriate cuttings.

Now attach a tunneling suppression factor of $e^{-2\pi/\alpha_w}$ to each effective vertex, and attach the growing part of the holy grail function to each bond. For example, in the "Higgs-only" example discussed in Sec. 2.2 the bond would be associated with[32] $\exp\left\{\frac{4\pi}{\alpha_w}\cdot\frac{3}{8}\left(\frac{E}{E_0}\right)^2\right\}$. So figs. 20a and 20b $\sim$ $\exp\left\{\frac{4\pi}{\alpha_w}\left[-1+\frac{3}{8}\left(\frac{E}{E_0}\right)^2\right]\right\}$ and $\exp\left\{\frac{4\pi}{\alpha_w}\left[-2+\frac{9}{8}\left(\frac{E}{E_0}\right)^2\right]\right\}$, respectively. The simple observation[5,56] is that the latter exponential reaches unity when the former is still tiny, $e^{-4\pi/3\alpha_w}$. In fact, iterating the same bond function, one finds that the chain consisting of an infinite number of $I\bar{I}$ pairs reaches unity when the one-instanton result is $e^{-2\pi/\alpha_w}$—the geometric mean of the few $\to$ few ($\sim e^{-4\pi/\alpha_w}$) and the many $\to$ many (~ 1) anomalous cross sections. Obviously this argument is independent of one's choice of bond function $B(E)$, so long as it grows with energy.

What is the consequence of this proposed breakdown of the dilute instanton gas approximation? In principle, the sum of all multiinstanton contributions could be either suppressed or unsuppressed. Zakharov guesses that they assemble into a geometric series, *e.g.*,

$$\begin{aligned}\sigma_{\not B} \;\sim\; &\exp\left\{\frac{4\pi}{\alpha_w}\left[-1+\frac{3}{8}\left(\frac{E}{E_0}\right)^2\right]\right\} \;-\; \exp\left\{\frac{4\pi}{\alpha_w}\left[-2+\frac{9}{8}\left(\frac{E}{E_0}\right)^2\right]\right\} \\ &+\; \exp\left\{\frac{4\pi}{\alpha_w}\left[-3+\frac{15}{8}\left(\frac{E}{E_0}\right)^2\right]\right\} \;-\; \cdots \qquad (4.3) \\ =\; &\tfrac{1}{2}e^{-2\pi/\alpha_w}\operatorname{sech}\left\{\frac{2\pi}{\alpha_w}\left[-1+\frac{3}{4}\left(\frac{E}{E_0}\right)^2\right]\right\} \;<\; e^{-2\pi/\alpha_w}\,,\end{aligned}$$

in which case B violation is never observable. The alternating signs in (4.3) presumably come from counting a Gaussian factor of i for each unstable mode

of the multiinstanton configuration. If this is eventually confirmed, it would paint a striking picture of the structure of the electroweak vacuum, or at least of the components thereof that couple to high-energy modes: a dense "liquid" of instantons as in QCD,[58] but in stark contrast to QCD, a liquid in which anomalous processes are exponentially suppressed at zero temperature.

In treating separately and additively the expansions about the configurations (4.1) and (4.2) (say), is one in fact guilty of double-counting? This is conceivable, as the two configurations are in the same topological class, but I believe the answer is no. The reason is that the expansion points (4.1) and (4.2), together with all tree-graph final-state corrections thereto, assemble into partial cross sections $\sim \exp\left(\frac{4\pi}{\alpha_w}F_1(E/E_{sphal})\right)$ and $\exp\left(\frac{4\pi}{\alpha_w}F_2(E/E_{sphal})\right)$, respectively, where F_1 and F_2 are *independent* holy grail functions satisfying $F_1(0) = -1$ and $F_2(0) = -2$. And the sum of two such functions *cannot* be reexpressed as a new such function with a modified F. Whether the *infinite* sum of such functions can be so expressed is, of course, anyone's guess.

In order to understand the effective Lagrangian approach of Refs. [5] and [56] a little better, let us see how to reproduce the leading-order Ringwald result in the Higgs-only model.[32,35,25] * As we saw earlier, on shell, the instanton acts like a pointlike vertex at which an arbitrary number n_h of Higgs lines meet, with strength $(2\pi^2\rho^2 v)^{n_h}$. So the on-shell instanton is mocked up by the nonrenormalizable effective interaction

$$\sum_{n_h} \frac{1}{n_h!}\left[\phi(x)\right]^{n_h}(2\pi^2\rho^2 v)^{n_h} \;=\; e^{2\pi^2\rho^2 v\phi(x)} \;. \tag{4.4}$$

The off-shell form factors are constructed through radiative corrections to these effective vertices.

* The more complicated case of gauge meson production is worked through in Ref. [56].

As fig. 20 suggests, the bond function $B(P_{tot})$ as a function of momentum P_{tot} flowing through the diagram is given by the following expression:**

$$\begin{aligned} B(P_{tot}) \;&=\; \mathrm{Im}\int d^4x\, e^{iP_{tot}\cdot x}\int_0^\infty \mathcal{D}\rho\,\mathcal{D}\rho'\, e^{-\pi^2(\rho^2+\rho'^2)v^2} \\ &\times \sum_{n_h}\frac{1}{n_h!}\Big[(2\pi^2\rho^2 v)(2\pi^2\rho'^2 v)\,\langle\phi(x)\phi(0)\rangle\Big]^{n_h} \;. \end{aligned} \tag{4.5}$$

Using the free-propagator approximation

$$\langle\phi(x)\phi(0)\rangle \;=\; \frac{1}{4\pi^2x^2} \;, \tag{4.6}$$

the fact that[56]

$$\mathrm{Im}\int d^4x\, e^{iP_{tot}\cdot x}\,\frac{1}{(x^2)^{n_h}} \;=\; \frac{i\pi^2 2^{4-2n_h}}{\Gamma(n_h-1)\Gamma(n_h)}\left(P_{tot}^2\right)^{n_h-2}\log(-P_{tot}^2) \;, \tag{4.7}$$

and the ever-useful Stirling's formula, one finds to leading exponential order,

$$B(P_{tot}) \;\sim\; \int_0^\infty \mathcal{D}\rho\,\mathcal{D}\rho'\,\exp\Big\{-\pi^2(\rho^2+\rho'^2)v^2+\left(\tfrac{27}{4}\pi^2\rho^2\rho'^2v^2P_{tot}^2\right)^{1/3}\Big\} \;. \tag{4.8}$$

The ρ integrations are performed in steepest descent as usual, and give

$$B(P_{tot}) \;\sim\; \exp\Big\{\frac{4\pi}{\alpha_w}\cdot\frac{3}{8}\Big(\frac{P_{tot}}{E_0}\Big)^2\Big\} \;, \tag{4.9}$$

correctly reproducing the leading-order Ringwald result for this model.[32]

4.2. A multi-instanton R-term calculation

The Zakharov-Maggiore-Shifman scenario is intriguing, but at this writing is yet to be bolstered by a compelling calculation. For one thing, it is based on nearest-neighbor two-body interactions, whereas at high energies the typical $I\bar{I}$ separation measured in units of ρ is small, and consequently next-nearest-neighbor as well as three- and higher-body forces should play a role. Furthermore, multiinstanton configurations such as fig. 20b admit a richer class

** To leading exponential order one can neglect the fact that two of the Higgs lines at each vertex are tied to the initial quanta, and one can likewise ignore the fermions.

of tree-graph corrections than does fig. 20a. Finally there is the question of how one cuts these diagrams to reveal purely B-violating amplitudes. Whether, when these issues are all incorporated, it will *still* be true that the multiinstanton contributions catch up to the one-instanton amplitude when the latter is tiny, is a completely open question.

The R-term method is a potentially useful tool for addressing these issues. As an illustration, let us calculate the overlap between the states (4.1) and (4.2) in Weinberg-Salam theory. To leading order, the independent path integration variables $A(x)$ and $A'(x)$ will be taken to be

$$A^{\mu a}(x) \longrightarrow A^{\mu a}_{\rm inst}(x;\xi_1,\rho_1) \tag{4.10}$$

and

$$A'^{\mu a}(x) \longrightarrow A^{\mu a}_{\rm inst}(x;\xi_2,\rho_2) + A^{\mu a}_{\rm inst}(x;\xi_3,\rho_3) + \bar{A}^{\mu a}_{\rm inst}(x;\xi_4,\rho_4)\,. \tag{4.11}$$

We are assuming from the outset that the choice of unity for the relative isospin orientations of the (anti)instantons is stationary. The initial-state phase factors $R^*(p_1)R^*(p_2)$ now consist of a sum of three terms, proportional to $e^{-iP_{\rm tot}\cdot(\xi_k-\xi_1)}$ with $k=2,3,4$. Thus there are actually three saddle-point calculations to be done, two of which ($k=2,3$) are identical by symmetry, while the third, $k=3$, turns out at the end to give a smaller answer. So we take $k=2$ in what follows.

We work in the center of mass frame $P_{\rm tot}=(E,\mathbf{0})$. The exponent to be minimized is then

$$\begin{aligned} W \;\simeq\; & -iE\cdot(\xi_{20}-\xi_{10}) - \frac{8\pi}{\alpha_{\rm w}} - \pi^2v^2(\rho_1^2+\rho_2^2+\rho_3^2+\rho_4^2) \\ & + \frac{96\pi^2}{g^2}\left[\frac{\rho_1^2\rho_2^2}{(\xi_{20}-\xi_{10}+i\epsilon)^4} + \frac{\rho_1^2\rho_3^2}{(\xi_{30}-\xi_{10}+i\epsilon)^4}\right] \\ & + S_{I\bar{I}}(\xi_2\rho_2;\xi_4\rho_4) + S_{I\bar{I}}(\xi_3\rho_3;\xi_4\rho_4) + S_{II}(\xi_2\rho_2;\xi_3\rho_3) + S_{II\bar{I}}(\xi_2\rho_2;\xi_3\rho_3;\xi_4\rho_4)\,. \end{aligned} \tag{4.12}$$

Here we have anticipated that the saddle point occurs when

$$\vec{\xi}_2-\vec{\xi}_1 \;=\; \vec{\xi}_3-\vec{\xi}_1 \;=\; \vec{\xi}_4-\vec{\xi}_1 \;=\; \mathbf{0} \tag{4.13}$$

by symmetry. The first two lines of (4.12) are the obvious generalization of Eq. (3.20). Note that, to the leading $(E/E_0)^{4/3}$ order to which we are working, there is no R-term contribution from the overlap of $A_{\rm inst}(x;\xi_1)$ and $\bar{A}_{\rm inst}(x;\xi_4)$, the reason being that when the second $\bar{\eta}$ tensor in Eq. (3.16) is swapped for an η, the polarization sum in (3.18) turns out to be proportional to $\omega_{\mathbf{k}}^2 - \mathbf{k}^2 = M_W^2 \ll \mathbf{k}^2$. The third line of (4.12) represents the 2-body and 3-body interactions amongst $A_{\rm inst}(x;\xi_2)$, $A_{\rm inst}(x;\xi_3)$ and $\bar{A}_{\rm inst}(x;\xi_4)$, the subscripts I ($\bar{I}$) standing for (anti)instanton. The $S_{I\bar{I}}$ interaction is given in Ref. [51] and contributes

$$\frac{96\pi^2}{g^2}\left[\frac{\rho_2^2\rho_4^2}{\left((\xi_{20}-\xi_{40})^2-i\epsilon\right)^2} + \frac{\rho_3^2\rho_4^2}{\left((\xi_{30}-\xi_{40})^2-i\epsilon\right)^2}\right] \tag{4.14}$$

in Minkowski continuation; neither S_{II} nor $S_{II\bar{I}}$ appears at the $(\rho/\Delta\xi)^4 \sim (E/E_0)^{4/3}$ order.

Rotating the ξ_0's to the imaginary axis consistent with the $i\epsilon$ prescriptions and switching variables to $\Delta_{kl}=\frac{1}{i}(\xi_{k0}-\xi_{l0})$, we can rewrite

$$\begin{aligned} W \;=\; & E\cdot\Delta_{21} - \frac{8\pi}{\alpha_{\rm w}} - \pi^2v^2\sum\rho_i^2 + \frac{96\pi^2}{g^2}\left\{\frac{\rho_1^2\rho_2^2}{\Delta_{21}^4} + \frac{\rho_1^2\rho_3^2}{\Delta_{13}^4} + \frac{\rho_2^2\rho_4^2}{\Delta_{42}^4} + \frac{\rho_3^2\rho_4^2}{\Delta_{34}^4}\right\} \\ & - \lambda E\cdot(\Delta_{21}+\Delta_{13}+\Delta_{42}+\Delta_{34}) + \mathcal{O}(\rho^6/\Delta^6) \end{aligned} \tag{4.15}$$

where λ is a Lagrange multiplier. The variational equations for the Δ_{kl} and λ then give

$$\begin{aligned} & \Delta_{21} = \kappa\left(\frac{\rho_1^2\rho_2^2}{1-\lambda}\right)^{1/5}\,,\quad \Delta_{13} = -\kappa\left(\frac{\rho_1^2\rho_3^2}{\lambda}\right)^{1/5}\,,\quad \Delta_{42} = -\kappa\left(\frac{\rho_2^2\rho_4^2}{\lambda}\right)^{1/5}\,, \\ & \Delta_{34} = -\kappa\left(\frac{\rho_3^2\rho_4^2}{\lambda}\right)^{1/5}\,,\quad \lambda \;=\; \frac{\left(\rho_1^{2/5}\rho_3^{2/5}+\rho_2^{2/5}\rho_4^{2/5}+\rho_3^{2/5}\rho_4^{2/5}\right)^5}{\left(\rho_1^{2/5}\rho_3^{2/5}+\rho_2^{2/5}\rho_4^{2/5}+\rho_3^{2/5}\rho_4^{2/5}\right)^5+\rho_1^2\rho_2^2} \end{aligned} \tag{4.16}$$

with $\kappa=(384\pi^2g^{-2}E^{-1})^{1/5}$. Eliminating these variables from (4.15) leaves a *bona fide* maximization problem in the ρ_i which must be solved numerically. But a lower bound on W can be had on the back of an envelope simply by

setting the ρ_i equal to one another. With this simplification one finds after a little algebra,

$$W_{\text{saddle}} > \frac{4\pi}{\alpha_w}\left[-2+4.43\left(\frac{E}{E_0}\right)^{4/3}+\mathcal{O}(E/E_0)^{6/3}\right], \quad E_0 = \sqrt{6}\pi\frac{M_W}{\alpha_w}. \quad (4.17)$$

Adding in the one-instanton result, Eq. (3.22), one therefore finds

$$\begin{aligned}\sigma_{\not B} \approx\ & f_1(E/E_0)\exp\left\{\frac{4\pi}{\alpha_w}\left[-1+\frac{9}{8}\left(\frac{E}{E_0}\right)^{4/3}+\cdots\right]\right\} \\ &+ f_2(E/E_0)\exp\left\{\frac{4\pi}{\alpha_w}\left[-2+4.43\left(\frac{E}{E_0}\right)^{4/3}+\cdots\right]\right\} \\ &+ \text{(higher multiinstanton contributions)},\end{aligned} \quad (4.18)$$

where the f_i are unknown prefactor functions. Notice that *if* one truncates the calculation at the leading $(E/E_0)^{4/3}$ order, the second exponential indeed catches up to the first when the first is still tiny. But will this phenomenon survive beyond leading order?

5. Initial-State Corrections

In this Section, we confront the third and final source of important corrections to $\sigma_{\not B}$ at sphaleron energies. These are the corrections due to the high-energy initial-state quanta,* which physical intuition[28] and explicit calculation[39,40] suggest should damp the growth of the anomalous cross section with energy (see however Ref. [29]). In general, corrections to the Ringwald-Espinosa calculation will involve both hard lines and soft lines interacting in a complicated way. In order to isolate the effect of the hard lines, we will not allow the multiplicity to grow large. Instead we will focus on an *exclusive* process, say $2 \to 3$ as pictured in fig. 21, in the limit that a lot of energy has been pumped into the system, so that all the $p_i \cdot p_j \gg m^2$. In Sec. 5.1 we will analyze the first correction to the Ringwald approximation of fig. 21; this correction is

* A technical point: the division between initial-state and final-state corrections is actually somewhat ambiguous, as it depends on one's choice of propagator in the instanton background.[59,36]

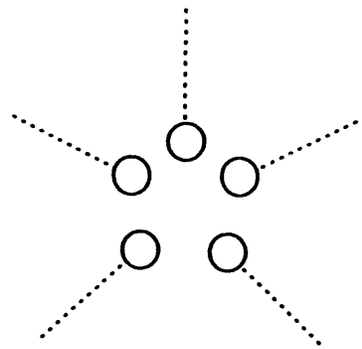

Fig. 21. A five-point function in Ringwald-Espinosa approximation.

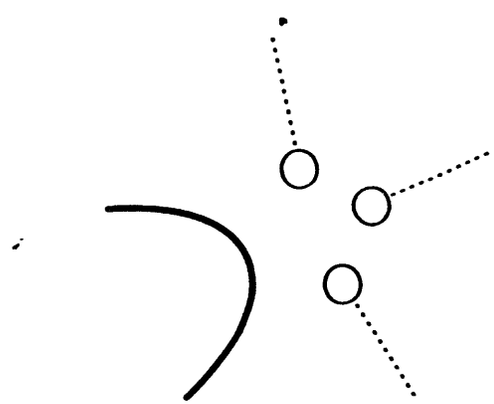

Fig. 22. The leading $\mathcal{O}(\alpha_w)$ multiplicative correction to fig. 21 (since two instanton factors of g^{-1} have been lost). The solid line is a propagator in the instanton background.

depicted in fig. 22, and involves a propagator insertion. The upshot is that, at sphaleron energies, fig. 22 is *bigger* than fig. 21 by a factor of $1/\alpha$. In Secs. 5.2-5.3, we will turn our attention to higher-order corrections involving loops, and show that these, too, must be taken into account, in contrast to loops involving soft particles which were seen to be unimportant. Suggestive arguments for exponentiation of the loop contributions will be reviewed. These surprising results, which are intimately related to the instanton's translational modes, can be found in two elegant articles by Mueller,[39,40] and in a recent paper by Li, McLerran, Voloshin and Wang.[29] The Lectures conclude (Sec. 5.4) with an early indication that—despite the importance of loops—hard-line corrections can nevertheless be treated *semiclassically.*[60]

5.1. Asymptotic analysis of propagators in instanton backgrounds

Our understanding of the simplest hard-line correction depicted in fig. 22 will require an asymptotic analysis of propagators $G(p,q)$ in instanton backgrounds in the limit $p\cdot q \to \infty$. In order to construct such propagators, we seek solutions of the small-fluctuations equation about $\phi_{\rm inst}$. The following analysis is model-independent, but for pedagogical clarity we will work in a generic scalar theory in an arbitrary dimension with interaction potential $V(\phi)$. $\phi_{\rm inst}$ will denote the *Minkowski continuation* of the instanton the theory is assumed to admit.

The small-fluctuations equation looks something like

$$\mathcal{D}_x^2\, G(x,y) \;\equiv\; \big(\Box_x + m^2 + V''(\phi_{\rm inst}(x))\big) G(x,y) \;\sim\; \delta(x-y)\,. \qquad (5.1)$$

Actually (5.1) as it stands has no solution, for $\mathcal{D}_x^2$ is not an invertible operator. The reason is that $\phi_{\rm inst}$ has zero modes z_i, which automatically obey

$$\mathcal{D}_x^2\, z_i(x) \;=\; 0\,. \qquad (5.2)$$

The z_i's are constructed as derivatives of $\phi_{\rm inst}$ with respect to the various collective coordinates, translational and otherwise. For later use, we digress momentarily to point out that (5.2) is the linearized version of the full nonlinear second-variation equation

$$\mathcal{D}_x^2\,\delta\phi \;+\; U(\delta\phi) \;=\; 0\,, \qquad U(\delta\phi) \;=\; V'(\phi_{\rm inst}+\delta\phi) - V'(\phi_{\rm inst}) - \delta\phi\, V''(\phi_{\rm inst}) \qquad (5.3)$$

whose solutions are the *finite* translations and/or other collective coordinate shifts, *e.g.*,

$$\delta\phi(x) \;=\; \phi_{\rm inst}(x+a) \;-\; \phi_{\rm inst}(x) \qquad (5.4)$$

for any a.

In order to make Eq. (5.1) well defined, the small fluctations about $\phi_{\rm inst}$ must be constrained to be orthogonal, either to the zero modes z_i themselves,[37] or more generally to an arbitrary set of functions f_i equal in number with the zero modes.[38] * The f_i are known as "Levine-Yaffe constraints" and their use is discussed at length in Ref. [38]. The associated Levine-Yaffe propagator G_f satisfies

$$\int dy\, G_f(x,y) f_i(y) \;=\; 0\,. \qquad (5.5)$$

The subscript f serves to remind us that the propagator depends explicitly on our choice of Levine-Yaffe constraints. The appropriate rewriting of Eq. (5.1) is then

$$\mathcal{D}_x^2\, G_f(x,y) \;=\; \delta(x-y) \;-\; \sum_{i,j} f_i(x) \big(\Omega^{-1}\big)_{ij}\, z_j(y) \qquad (5.6)$$

where Ω is the overlap matrix,

$$\Omega_{ij} \;=\; \int dx\, f_i(x) z_j(x)\,. \qquad (5.7)$$

By inspection, (5.6) is consistent with the orthogonality conditions

$$0 \;=\; \int dx\, z_i(x)\, \mathcal{D}_x^2\, G_f(x,y) \;=\; \int dy\, \mathcal{D}_x^2\, G_f(x,y)\, f_i(y) \qquad (5.8)$$

required by Eqs. (5.2) and (5.5). The only technical restriction on one's choice of Levine-Yaffe constraints comes from (5.6), namely that Ω be invertible.

---

* In many models, taking $f_i \equiv z_i$ is a particularly poor choice to make, as the resulting propagator has *double* poles on the mass shell which renders the LSZ amputation procedure meaningless and plagues perturbation theory with infinities.[37,38]

In general, $G_f(p,q)$ will have poles on both mass shells,[38] p^2 or $q^2 \to m^2$. As it is preferable to work with smoother functions, we define amputated momentum-space propagators

$$\bar{G}_f(p,q) \;=\; (p^2-m^2)\cdot G_f(p,q)\cdot(q^2-m^2)\,, \tag{5.9}$$

in terms of which Eq. (5.6) can be recast as the integral equation

$$\begin{aligned}\bar{G}_f(p,q) \;-\; &\int dk\, V''\big(\phi_{\rm inst}(p-k)\big)\,\frac{1}{k^2-m^2+i\epsilon}\,\bar{G}_f(k,q)\\ &=\; -(2\pi)^D(q^2-m^2)\delta(p+q) \;+\; f_i(p)\,\big(\Omega^{-1}\big)_{ij}\,z_j(q)(q^2-m^2)\,.\end{aligned} \tag{5.10}$$

We are interested in $\bar{G}_f$ in the kinematic regime where $p\cdot q \to \infty$ while p^2 and q^2 remain on or near mass shell, $p^2 \sim q^2 \sim m^2$. Notice that these limits are mutually inconsistent in Euclidean space (they violate the triangle inequality) but are perfectly sensible in Minkowski space. Unfortunately, in most theories momentum-space propagators in instanton backgrounds are not known in closed form, so we must instead analyze the defining Eq. (5.10). In this kinematic regime, we can drop the first term on the right-hand side of (5.10) and concentrate on the second term. To see how it behaves, focus on the translational zero modes of the theory, $z_\mu \propto g\partial_\mu\phi_{\rm inst}$, where the g here just compensates the g^{-1} in $\phi_{\rm inst}$. Furthermore, choose Levine-Yaffe constraints of the form $f_\mu \propto \partial_\mu f$ where f is a scalar function, $f = f(x^2)$, that is assumed to fall off sufficiently rapidly at large x^2 that its Fourier transform has no pole on mass shell. So this term grows like $p\cdot q$ from the dot products of the Fourier-transformed gradients. Other potential zero modes in the theory grow less rapidly as functions of $p\cdot q$ and can therefore be ignored for present purposes.

We therefore infer from (5.10) that $\bar{G}_f(p,q)$ grows *at least* as rapidly as $p\cdot q$. This is not surprising, for the following reason. Given any solution to the inhomogeneous Eq. (5.10), one can add an arbitrary admixture of the amputated translational zero mode projection operator

$$g^2 p\cdot q\,\phi_{\rm inst}(p)\,\phi_{\rm inst}(q)\,(p^2-m^2)(q^2-m^2) \tag{5.11}$$

which, from (5.2), solves the homogeneous equation gotten by setting the right-hand side of (5.10) to zero. This, too, grows like $p\cdot q$. The specific amount of (5.11) that one needs to add is fixed implicitly by the Levine-Yaffe orthogonality condition (5.5).

Experience with differential and integral equations leads us to look for the *most singular possible behavior* of $\bar{G}_f(p,q)$ as a function of $p\cdot q$; subleading contributions can then be constructed by an interative procedure. Mueller suggests that in general one can do a little better than $p\cdot q$, namely $p\cdot q\log p\cdot q$, by taking[39]

$$\bar{G}_f(p,q) \;\propto\; g^2 p\cdot q\log\big[(p+q)^2+i\epsilon\big]\phi_{\rm inst}(p)\phi_{\rm inst}(q)(p^2-m^2)(q^2-m^2)\,. \tag{5.12}$$

As before, the g^2 compensates the two factors of g^{-1} carried by the instantons. We have explicitly exhibited the $i\epsilon$ prescription inside the logarithm that allows rotation back to Euclidean space where propagators in the instanton background are originally defined.

To justify Mueller's ansatz (5.12), we should plug this expression into the left-hand side of (5.10) and verify directly that the result is less singular than the $p\cdot q\log p\cdot q$ behavior we are starting with.* Let us do so, noting that if under the integral we had $\log\big[(p+q)^2+i\epsilon\big]$ instead of $\log\big[(k+q)^2+i\epsilon\big]$, the left-hand side of (5.10) would vanish identically due to the zero-mode condition (5.2). What remains, then, is the *difference* of the logarithms, namely

$$\begin{aligned}-\int dk\, V''\big(\phi_{\rm inst}(p-k)\big)\,&\frac{g^2\,k\cdot q}{k^2-m^2+i\epsilon}\,\log\frac{(k+q)^2+i\epsilon}{(p+q)^2+i\epsilon}\\ &\times\;\phi_{\rm inst}(k)\phi_{\rm inst}(q)(k^2-m^2)(q^2-m^2)\\ =\int dk\, V''\big(\phi_{\rm inst}(p-k)\big)\,&k\cdot q\,\phi_{\rm inst}(k)\,\log\frac{(k+q)^2+i\epsilon}{(p+q)^2+i\epsilon}\\ &\times\;\big(\text{smooth function of } q^2\big)\,.\end{aligned} \tag{5.13}$$

* The following somewhat lengthy discussion through Eq. (5.24) is more straightforward than, and is complementary to, the argument Mueller gives in Sec. 4.3 of Ref. [39].

To make progress, we invoke the spectral decomposition of the Minkowski-continued instanton, Eq. (3.50). Polynomials in $\phi_{\rm inst}$ also admit such decompositions; thus

$$V''\big(\phi_{\rm inst}(p-k)\big) \;=\; \int_0^\infty \mathrm{d}(\tilde\mu^2)\,\frac{i\tilde\sigma(\tilde\mu^2)}{(k-p)^2-\tilde\mu^2+i\epsilon} \tag{5.14}$$

for some new spectral weight $\tilde\sigma$. The specific form of the spectral weights will not be needed. We now insert (3.50) and (5.14) into (5.13) and switch orders of integration so that the μ^2 and $\tilde\mu^2$ integrals are to be done last, while the inner k integral becomes

$$\int dk\,\frac{1}{(k-p)^2-\tilde\mu^2+i\epsilon}\,\frac{k\cdot q}{k^2-\mu^2+i\epsilon}\,\log\frac{(k+q)^2+i\epsilon}{(p+q)^2+i\epsilon}\,. \tag{5.15}$$

Perhaps Eq. (5.15) can be carried out in closed form using dilogarithms and related special functions, but since all we are after is the leading $p\cdot q$ behavior we can take an easier route. We work in a collinear frame[†]

$$p \;=\; (\sqrt{|\mathbf{p}|^2+m_1^2}\,,0,0,|\mathbf{p}|)\,,\quad q \;=\; (-\sqrt{|\mathbf{q}|^2+m_2^2}\,,0,0,|\mathbf{q}|) \tag{5.16}$$

where $|\mathbf{p}|$ and $|\mathbf{q}|$ are assumed to be enormous, $|\mathbf{p}|$ and $|\mathbf{q}| \gg m$, but the virtualities m_1^2 and m_2^2 are small, of order m^2. We also use lightcone coordinates, Eq. (2.25), in terms of which p^+ and $-q^-$ are the large components, and the denominators in (5.15) become

$$k^2-\mu^2+i\epsilon \;=\; k^+k^- - \mathbf{k}_\perp^2-\mu^2+i\epsilon \tag{5.17}$$

and so forth. The k integral (5.15) is formally divergent but the original expression (5.13) is not, so we introduce an ultraviolet regulator Λ on the $\mathbf{k}_\perp$ integration, taking

$$\int dk \;\to\; \int^\Lambda d\mathbf{k}_\perp \int dk^-dk^+\,. \tag{5.18}$$

The cutoff Λ plays no role in what follows.

[†] We will use the word 'collinear' to mean that the *three*-momenta are aligned.

Now consider the k^+ integration in Eq. (5.15). It is easy to check that it vanishes unless

$$0 \;<\; k^- \;<\; -q^-\,, \tag{5.19}$$

since otherwise the singularities all lie on the same half of the complex k^+ plane and the contour can be closed so as to include no singularities, giving zero. An identical analysis of the k^- integration implies

$$0 \;<\; k^+ \;<\; p^+\,. \tag{5.20}$$

These inequalities suggest that we switch to the dimensionless rescaled variables α and β

$$k^- \;=\; -\alpha q^-\,,\qquad k^+ \;=\; \beta p^+\,, \tag{5.21}$$

which run from 0 to 1. In terms of these variables, Eq. (5.15) becomes

$$\begin{aligned}\tfrac{1}{2}\int_0^\Lambda d\mathbf{k}_\perp\int_0^1 d\alpha\,d\beta\;&\frac{\beta+\alpha m_2^2 s^{-1}}{(\beta-1)(\alpha-m_1^2s^{-1})-(\mathbf{k}_\perp^2+\tilde\mu^2)s^{-1}+i\epsilon}\\ &\times\;\frac{1}{\alpha\beta-(\mathbf{k}_\perp^2+\mu^2)s^{-1}+i\epsilon}\\ &\times\;\log\big[(1-\alpha)\beta+\mathcal{O}(s^{-1})-i\epsilon\big]\end{aligned} \tag{5.22}$$

with $s=-p^+q^-\simeq -2p\cdot q$.

One analyzes the asymptotic behavior of (5.22) as a function of s by seeing where the integrand can blow up. The dominant singularity when $s\to\infty$ is a linear divergence at $\alpha=0$, so let us set $\alpha=0$ inside the logarithm, thereby throwing out contributions subleading in s. The resulting α integration is elementary, giving the $s\to\infty$ result

$$\begin{aligned}\frac{s}{2}\int^\Lambda d\mathbf{k}_\perp\int_0^1 d\beta\;&\frac{\beta\log\beta}{\beta(1-\beta)m_1^2-\mathbf{k}_\perp^2-(1-\beta)\mu^2-\beta\tilde\mu^2+i\epsilon}\\ &\times\;\log\Big[\frac{\beta-1}{\beta}\,\frac{\mathbf{k}_\perp^2+\mu^2-i\epsilon}{(\beta-1)m_1^2+\mathbf{k}_\perp^2+\tilde\mu^2-i\epsilon}\Big]\,.\end{aligned} \tag{5.23}$$

The linear divergence in α is responsible for the explicit factor of s outside, after which we were able safely to take $s\to\infty$ inside the integral, with no further divergences.

Fortunately, we need not push the calculation any further, as Eq. (5.23) establishes the earlier claim that the leading $p \cdot q \log p \cdot q$ behavior cancels out when (5.12) is stuffed into (5.10), leaving a less singular expression that scales like $p \cdot q$, stripped of the logarithm. This justifies (not very rigorously) Mueller's assertion that, in general,

$$G_f(p,q) \;=\; cg^2\rho^2\, p\cdot q \log(p\cdot q)\phi_{\rm inst}(p)\phi_{\rm inst}(q) \;+\; \cdots\;, \qquad (5.24)$$

where c is a model-dependent numerical constant, ρ^2 is inserted for dimensional reasons, and the dots stand for subleading terms in $p \cdot q$. The ansatz (5.24) has been explicitly verified in 4-dimensional gauge theory[39] and in the 2-dimensional $O(3)$ sigma model[29,61] ; in both cases c is negative.

Comparing Eq. (5.24) to the Ringwald-Espinosa approximation $\phi_{\rm inst}(p)\times \phi_{\rm inst}(q)$, we see that the propagator gives a multiplicative correction of $cg^2\rho^2\, p\cdot q \log p\cdot q$, which is a large number, of order $\alpha^{-1}\log\alpha^{-1}$, at sphaleron energies. As Mueller notes,[39] the $\log\alpha^{-1}$ actually drops out when one considers propagator insertions such as fig. 22, summed over all permutations of external momenta. Setting

$$p_i \cdot p_j \;=\; \theta_{ij}\cdot s\;, \qquad (5.25)$$

where the 'angles' θ_{ij} are of order unity, we see that the order $s\log s$ pieces cancel by overall momentum conservation, since

$$\sum p_i\cdot p_j \;=\; \tfrac{1}{2}\Big(\sum p_i\Big)^2 \;-\; \tfrac{1}{2}\sum m_i^2 \;=\; -\,\tfrac{1}{2}\sum m_i^2 \;\ll\; s\;. \qquad (5.26)$$

The net contribution of fig. 22 is therefore a multiplicative correction

$$cg^2\rho^2 \sum_{\langle ij\rangle} p_i\cdot p_j \log\theta_{ij}\;. \qquad (5.27)$$

5.2. Loop graphs, naive exponentiation of Mueller's single-propagator-insertion result, and a major caveat

We will now see that when higher-order diagrams are taken into account, including loops, the apparent effect is that Eq. (5.27) exponentiates, giving an order $\exp(1/\alpha)$ correction to Ringwald, just like final-state tree-graph contributions. A qualitative all-orders argument for exponentiation was first given by Mueller in Sec. 4 of Ref. [40]. Here we will elaborate a rather different, and deceptively simple, argument given by Li, McLerran, Voloshin and Wang.[29] The contrast between the exponentiation of initial-state versus final-state corrections is striking. In the case of the final state, as we saw, exponentiation reflects the traditional relation between connected and disconnected graphs, the graphs in question being tree-level R-term diagrams. In contrast, in the initial state, exponentiation seems to come about from diagrams containing more and more loops. A significant caveat to initial-state exponentiation will also be discussed.

We focus first on loop corrections to the propagator in the instanton background $G_f(p,q)$. Examples of the diagrams we will estimate are depicted in fig. 23. Evidently these are loop graphs of a special type: they can all be pictured as *squared trees* in which the leaves from each tree are tied together in all possible ways. An example of a loop graph that is *not* of this type is the double bubble shown in fig. 24; such diagrams will be discussed in Sec. 5.3. Following Li *et al.* [29] we will evaluate the sum of all squared-tree diagrams subject to two kinematical approximations:

(i) All lines in these diagrams will be the full propagators G_f in the instanton background, except for the lines connecting the two trees; these will be replaced by the asymptotic piece of G_f given in Eq. (5.24). This replacement is justified if one imagines that the number of bifurcations of the tree branches is relatively small, and that the bulk of the momentum transfer across the diagram occurs at the joining of the leaves of the two trees. If we denote the incoming and outgoing momenta across the leaves by k_i and l_i, respectively, while the external "tree-trunk" momenta are p and q, the assumption is that

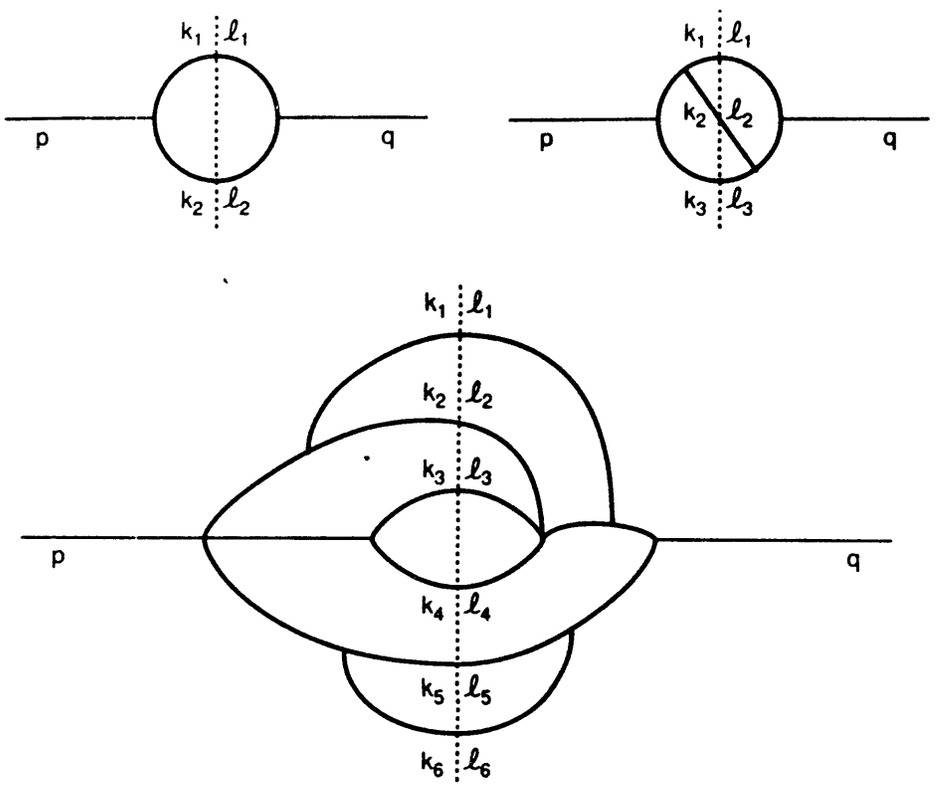

Fig. 23. Loop corrections to the propagator in the instanton background. These loop graphs can all be viewed as "squared trees," as the dotted line makes clear.

the dot products $k_i \cdot l_j$ are all large, of order s, while $k_i \cdot p$ and $l_i \cdot q$ are much smaller, say of order m^2. That is, the k_i and l_i are assumed to be roughly proportional to p and q, respectively, up to small perpendicular components. This partitioning of momentum transfer will be explained in Sec. 5.3 using rapidity

ordering arguments.

(ii) Furthermore, by the same reasoning, the factor of $k_i \cdot l_j \log k_i \cdot l_j$ that appears in the asymptotic propagator (5.24) across each of the leaves will be approximated by $\frac{1}{2} k_i^+ l_j^- \log p \cdot q$ (assuming the collinear frame (5.16) for p and q) so that we are only working to "leading logs." The important simplification is that with this substitution, the asymptotic propagator (5.24) factorizes:

$$G_f(k_i, l_j) \simeq \left(\varepsilon k_i^+ \phi_{\text{inst}}(k_i)\right)\left(\varepsilon l_j^- \phi_{\text{inst}}(l_j)\right) , \qquad \varepsilon = \left(\tfrac{1}{2} c g^2 \rho^2 \log p \cdot q\right)^{1/2} . \tag{5.28}$$

Fig. 25 depicts the sum of the $(n-1)$-loop squared-tree graphs that appear at the n-leaf level. The shaded blobs here represent the sum of all possible tree-level branchings of the external legs into n leaves. Thanks to Eq. (5.28), the sum of these graphs approximately factorizes as indicated in the drawing. In position space, each cross on the left or right half stands for $i\varepsilon \frac{\partial}{\partial x^-} \phi_{\text{inst}}(x)$ or $i\varepsilon \frac{\partial}{\partial y^+} \phi_{\text{inst}}(y)$, respectively, while the $n!$ counts the number of ways of tying the two halves together to form the multiloop graph.

Remarkably, as Li *et al.* point out, a closed-form expression is available almost trivially for the sum of tree-level one-point functions, which we draw afresh in fig. 26. In general, sums of tree graphs solve a classical equation of motion, which in the present case is the nonlinear second-variation Eq. (5.3). As per Eq. (5.4), the solution with the correct order ε term is the finite translation

$$\delta\phi(x) = \phi_{\text{inst}}(x + i\varepsilon n^-) - \phi_{\text{inst}}(x) \tag{5.29}$$

where $n^\pm$ is the vector $(1, 0, 0, \pm 1)$. The ε^n Taylor coefficient of $\delta\phi$ is $\frac{1}{n!}(i\varepsilon)^n \frac{\partial^n}{\partial (x^-)^n} \phi_{\text{inst}}(x)$. So the product depicted in fig. 25 is

$$n! \times \frac{1}{n!}(i\varepsilon)^n \frac{\partial^n}{\partial (x^-)^n} \phi_{\text{inst}}(x) \times \frac{1}{n!}(i\varepsilon)^n \frac{\partial^n}{\partial (y^+)^n} \phi_{\text{inst}}(y) . \tag{5.30}$$

Note that the Ringwald approximation just corresponds to taking $n = 0$ in (5.30). Adding it in and summing on n gives the exponentiated result[40,29]

$$e^{c g^2 \rho^2 p \cdot q \log p \cdot q} \, \phi_{\text{inst}}(p) \phi_{\text{inst}}(q) , \tag{5.31}$$

where we have transformed back to momentum space and replaced $\frac{1}{2}p^+q^-$ by $p \cdot q$.

We can now estimate the hard initial-state gauge propagator contribution to the holy grail function in the richer physical circumstance that the final-state multiplicity is allowed to grow large as per Eqs. (2.17) and (2.20). For concreteness, the process we have in mind is

$$W + W \to 9\bar{q} + 3\bar{l} + n_W \times W + n_Z \times Z + n_h \times \phi \qquad (5.32)$$

The dominant instanton size ρ will be given by Eqs. (2.18) and (2.20) so that the exponent in (5.31) scales like $\alpha_w^{-1}(E/E_0)^{10/3}$ up to logarithms. Since $c < 0$, the leading initial-state contribution has the form of an exponential suppression. The 10/3 power is to be compared with the 6/3 effect of soft final-state gauge propagator insertions[44–46] as depicted in fig. 12, and with the 8/3 power[59] for the "hard-soft" corrections due to propagators that tie an initial to a final gauge leg. The dominant number of loops contributing to (5.31) can be read off from the exponent and is

$$\langle n_{\text{loop}} \rangle \sim g^2 \rho^2 E^2 \qquad (5.33)$$

neglecting logarithms and numerical constants. Of course, the validity of the entire analysis requires that the momentum transfer across the leaves is large,

$$\rho^2 \left(\frac{E}{\langle n_{\text{loop}} \rangle} \right)^2 \gg 1 \,. \qquad (5.34)$$

Combining these two conditions gives[40]

$$\left(\frac{E}{E_{\text{sphal}}} \right)^{10/3} \ll 1 \qquad (5.35)$$

which is equivalent to the small parameter (3.23) that enters into the analysis of the exponentiation of final-state corrections.

Despite the exponential form of Eq. (5.31), even when $E \ll E_{\text{sphal}}$ exponentiation for hard initial-state corrections is on *much shakier footing* than for

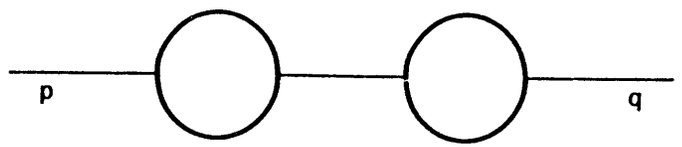

Fig. 24. A loop correction to the propagator that is not a squared tree.

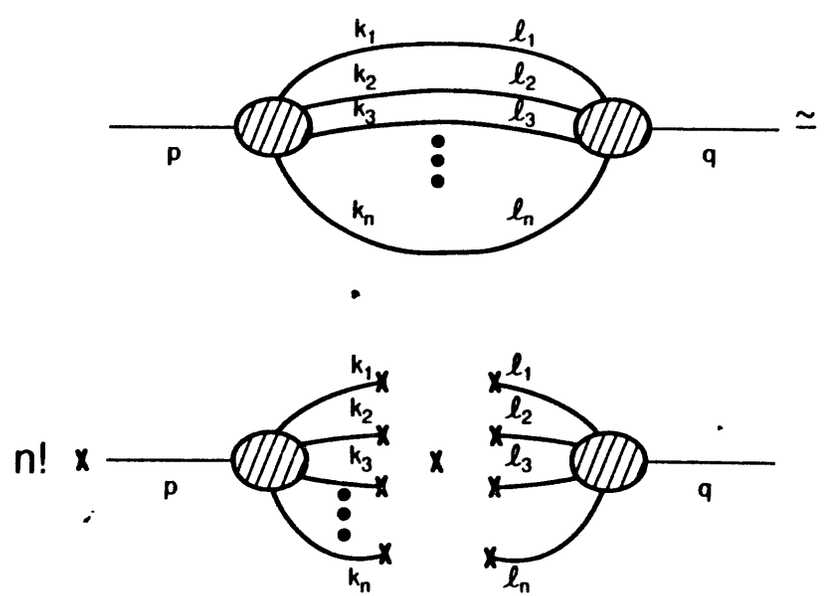

Fig. 25. The approximate factorization equation for squared trees. The shaded blobs represent the sum of all possible tree-level branchings.

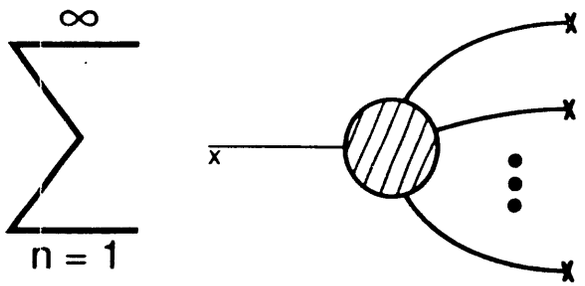

Fig. 26. The left-hand side of the factorized squared-tree graphs.

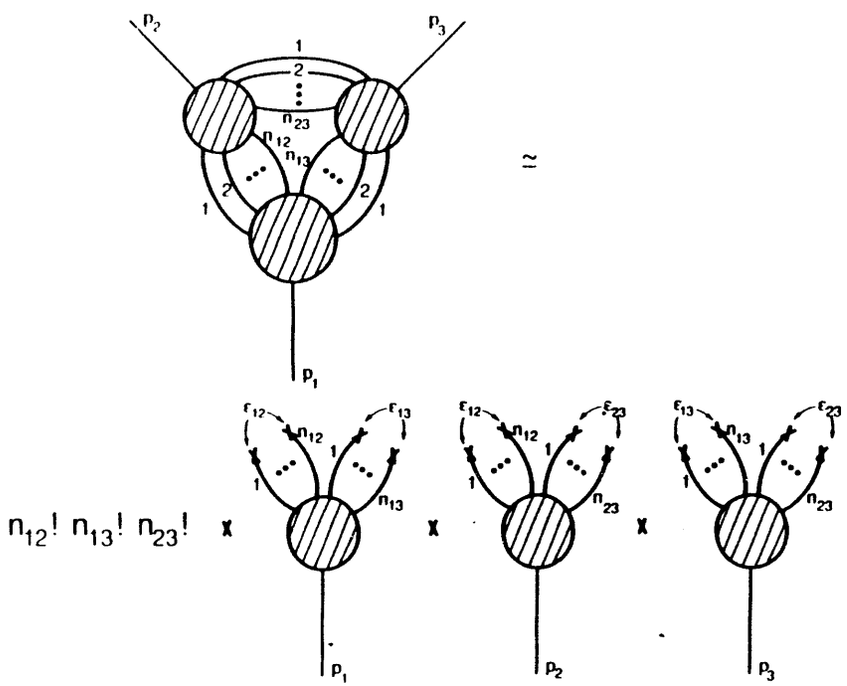

Fig. 27. The factorization equation for "cubed trees."

soft final-state corrections, where we found it to be rigorously true. The reason is the general observation that in summing Taylor series for decreasing exponentials with large negative exponents, one runs the risk of throwing out terms that are formally subleading at each order, but which sum to an unsuppressed result. A transparent example is the function

$$e^{-\alpha s} + \frac{1}{1-\alpha} = \sum_{n=0}^{\infty} \alpha^n \left[\frac{(-s)^n}{n!} + 1 \right] . \tag{5.36}$$

When $s \to \infty$, a leading asymptotic analysis, such as the one that culminated in Eq. (5.31), would have us drop the '1' inside the brackets at each order in perturbation theory, and conclude erroneously that the total answer is exponentially suppressed, rather than order unity. In their analysis of the 2-dimensional $O(3)$ sigma model, Li *et al.* suggest that precisely such an error is being made in the analysis leading up to Eq. (5.31), when this expression is applied in the kinematic region where the exponent is negative.[29]

Having noted this major caveat, let us nevertheless press on, and see how the method of Li *et al.* for estimating loop corrections to the propagator can be extended to multipoint functions involving only hard lines. Fig. 27 depicts a class of loop contributions to the 3-point function $G(p_1, p_2, p_3)$ (4-point and higher-point functions are harder to draw). The indicated diagrams are the sum of "cubed trees" in which n_{12} leaves connect the p_1 and p_2 trees, n_{13} leaves connect the p_1 and p_3 trees, and n_{23} leaves connect the p_2 and p_3 trees. The product of factorials reflects the number of possible tyings for a given choice of n_{ij}. As before, the leaf momenta k_i, l_i and r_i are assumed to be largely proportional to p_1, p_2 and p_3, respectively. For more than two particles a collinear frame such as (5.16) is no longer available so light-cone coordinates are not useful. Instead we will make the factorized leading-log approximation valid for 4-momenta with large components but small virtualities,

$$k_i \cdot l_j \log k_i \cdot l_j \simeq \frac{k_{i0} l_{j0}}{p_{10} p_{20}} p_1 \cdot p_2 \log p_1 \cdot p_2 \tag{5.37}$$

and so forth.

By the same reasoning as for the propagator, the first diagram on the right-hand side of fig. 27 is given by the $(\varepsilon_{12})^{n_{12}} \cdot (\varepsilon_{13})^{n_{13}}$ Taylor coefficient of the function

$$\delta\phi_1(x^\mu) \;=\; \phi_{\rm inst}\big(x^\mu + i(\varepsilon_{12}+\varepsilon_{13})\delta^{\mu 0}\big) \;-\; \phi_{\rm inst}(x^\mu) \tag{5.38}$$

with

$$\varepsilon_{ij} \;=\; \Big(cg^2\rho^2 \frac{p_i\cdot p_j}{p_{i0}p_{j0}} \log p_i\cdot p_j\Big)^{1/2} . \tag{5.39}$$

So the right-hand side of fig. 27 works out to

$$\begin{aligned}\sum_{n_{12}=0}^{\infty}\sum_{n_{13}=0}^{\infty}\sum_{n_{23}=0}^{\infty} n_{12}!n_{13}!n_{23}! \frac{(i\varepsilon_{12})^{n_{12}}(i\varepsilon_{13})^{n_{13}}}{n_{12}!n_{13}!} \frac{\partial^{n_{12}+n_{13}}}{\partial(x_0)^{n_{12}+n_{13}}}\phi_{\rm inst}(x) \\ \times \frac{(i\varepsilon_{12})^{n_{12}}(i\varepsilon_{23})^{n_{23}}}{n_{12}!n_{23}!} \frac{\partial^{n_{12}+n_{23}}}{\partial(y_0)^{n_{12}+n_{23}}} \\ \times \phi_{\rm inst}(y) \times \frac{(i\varepsilon_{13})^{n_{13}}(i\varepsilon_{23})^{n_{23}}}{n_{13}!n_{23}!} \frac{\partial^{n_{13}+n_{23}}}{\partial(z_0)^{n_{13}+n_{23}}}\phi_{\rm inst}(z) ,\end{aligned} \tag{5.40}$$

where in order to extend the summations on the n_{ij} down to zero we have added in the cases where one or more of the trees is treated in Ringwald approximation. These summations individually exponentiate as before, and give the approximate result which is most conveniently written in momentum space,[40]

$$G(p_1,p_2,\cdots,p_n) \;\simeq\; e^{cg^2\rho^2\sum_{(ij)} p_i\cdot p_j \log p_i\cdot p_j}\phi_{\rm inst}(p_1)\phi_{\rm inst}(p_2)\cdots\phi_{\rm inst}(p_n) , \tag{5.41}$$

generalizing trivially from 3-point to n-point functions involving only hard quanta.

5.3. Rapidity ordering and the suppression of other loop diagrams

In this subsection we look at loop corrections to the propagator such as fig. 24 that *cannot* be viewed as squared trees and explain why, at any *fixed* order in the loop expansion, their contribution is subleading in energy. Whether they nevertheless contribute significantly to $\sigma_{\rm tot}$ is not currently known, but it is at least plausible that they do not. Similar statements apply to 3-point and higher-point functions involving hard lines. The basic ideas of this subsection can be found in the paper of Li, McLerran, Voloshin and Wang.[29]

In order to estimate the size of graphs, we first need to establish some basic principles governing the flow of momentum in multiperipheral diagrams. In the process of laying this groundwork, we will better understand the kinematic assumptions made in the previous subsection, namely why the "leaf momenta" were taken to be approximately parallel to the external momenta, and why the bulk of the momentum transfer happened in the middle of the graphs, across the leaves.

Consider a particle propagating in Minkowski space undergoing numerous interactions of the sort depicted in fig. 28. The meaning of these emitted lines is quite general: they can represent real on-shell particles, or virtual quanta that will undergo further interactions, or, what is particularly germane to our purposes, Minkowski-continued instantons. The important point in common is that the emitted lines must admit spectral representations with Feynman $i\epsilon$ prescriptions. We will assume the collinear frame (5.16) for the external momenta p and q and work in lightcone coordinates as before. Thus $p^+ \gg 0$ and $q^- \ll 0$, with all other components essentially zero.

The following inequalities are easily proved:

$$0 \simeq p^- > k_1^- > \cdots > k_n^- > q^- \tag{5.42}$$

and

$$p^+ > k_1^+ > \cdots > k_n^+ > q^+ \simeq 0 . \tag{5.43}$$

That is to say, all regions of the intermediate momenta k_i that are not consistent with these inequalities give vanishing contributions to the propagation.

To prove (5.42), consider the k_1^+ integral from fig. 28,

$$\begin{aligned}\int dk_1^+ \frac{V(p,k_1,k_2)}{\big((k_1^+-p^+)(k_1^- - p^-) - \mathbf{k}_1^{\perp 2} - \mu^2 + i\epsilon\big)\big(k_1^+k_1^- - \mathbf{k}_1^{\perp 2} - \mu^2 + i\epsilon\big)} \\ \times \frac{1}{(k_1^+-k_2^+)(k_1^- - k_2^-) - (\mathbf{k}_1^\perp - \mathbf{k}_2^\perp)^2 - \mu^2 + i\epsilon} ,\end{aligned} \tag{5.44}$$

with $V(p, k_1, k_2)$ summarizing the polynomial interactions at the two vertices (if any), which are irrelevant to what follows. Locating the singularities in the complex k_1^+ plane, we see that (5.44) vanishes if

$$\text{sgn}(k_1^-) = \text{sgn}(k_1^- - p^-) = \text{sgn}(k_1^- - k_2^-)\,, \qquad (5.45)$$

since in this event the poles all lie on the same half-plane and the contour can be closed in the opposite direction. There are two cases to examine. First, suppose $k_1^- < 0$. Then (5.45) implies that $k_2^- < k_1^-$ necessarily. The k_2^+ integral then gives $k_3^- < k_2^-$ by identical reasoning, and so forth. In this way the inequality (5.42) is reproduced. Alternatively, if one assumes $k_1^- > 0$, the same reasoning leads to $k_1^- < k_2^- < \cdots < k_n^-$ until finally the k_n^+ integration gives zero, killing this possibility. The k^+ inequality (5.43) is proved in the same way, starting from the opposite end. Eqs. (5.42)-(5.43) imply "rapidity ordering" since obviously the same chain of inequalities applies to the rapidity variables $y_i = \log|k_i^+/k_i^-|$. An immediate physical consequence of these inequalities is that a propagating particle either monotonically loses or monotonically gains energy from repeated interactions with the instanton; the energy cannot oscillate.

Fig. 29 follows the characteristic 4-momentum of a particle as this quantity degrades from p to q subject to the rules of rapidity ordering. The intermediate momentum k needs to stay near the lightcone at all times since otherwise there are large denominators suppressing fig. 28. But the lightcone is a three-dimensional surface, whereas actually, to be consistent also with the inequalities (5.42) and (5.43), k must closely track the *one*-dimensional path shown in the figure. In particular, $k^\perp$ remains small throughout. It is now evident why in the previous subsection we were justified in taking the "leaf momenta" k_i and l_j to be roughly parallel to the external momenta p and q, respectively. Although this picture of 4-momentum uniformly degrading from p to 0, turning the corner, then building up from 0 to q was derived in the collinear frame (5.16), it is obviously frame independent.

The inequalities (5.42) and (5.43) together with fig. 29 imply the stronger condition that can be termed "s multiplication" across a high-energy line. By

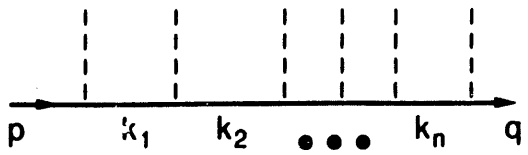

Fig. 28. A propagating particle undergoing numerous interactions with (for example) a Minkowski-continued instanton.

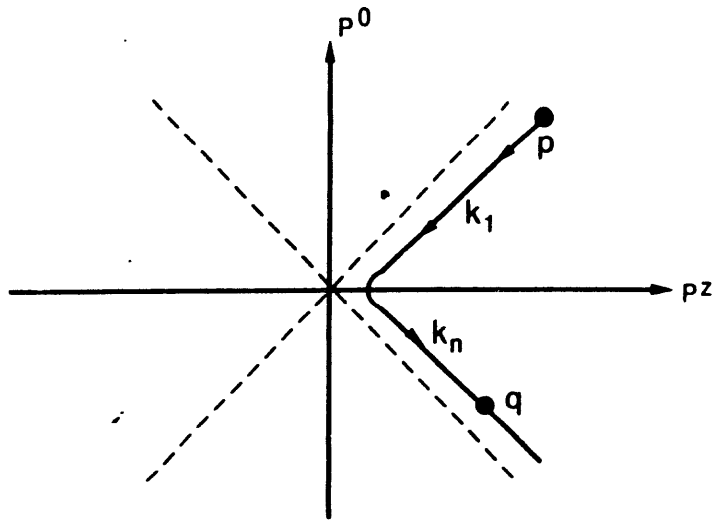

Fig. 29. This is how the momentum of the propagating particle of fig. 28 degrades from p to q. The momentum stays near the light cone at all times, and is first proportional to p, then to q after rounding the corner.

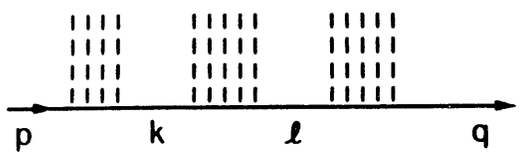

Fig. 30. Momentum degradation, split arbitrarily into three stages, to illustrate the concept of "s multiplication."

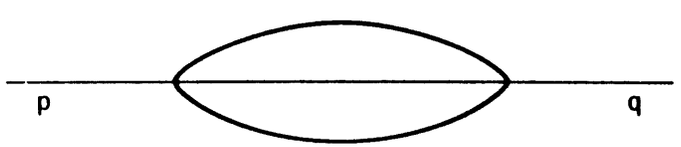

Fig. 31. A squared-tree graph that appears at the same order in perturbation theory as fig. 24.

this we intend the following. Let us subdivide the propagating line in fig. 28 into an arbitrary number of segments, as illustrated in fig. 30. For the ith segment, form the quantity s_i by dotting together the incoming and outgoing segment momenta. We will need to assume that there are only two energy scales in the problem, a large energy $\sim \sqrt{p \cdot q}$, and a small energy μ given by a typical mass, or typical offshellness $\sim |\mathbf{k}^\perp|$, or perhaps an instanton scale ρ^{-1} (whichever is larger). Then s multiplication is the statement that

$$\prod_i \frac{s_i}{\mu^2} \sim \text{const.} \times \frac{p \cdot q}{\mu^2} \,. \tag{5.46}$$

For example, the left-hand side of (5.46) applied to fig. 30 works out to

$$\mu^{-8}(\tfrac{1}{2}p^+k^-)(\tfrac{1}{2}k^+l^- + \tfrac{1}{2}k^-l^+ - \mathbf{k}^\perp \cdot \mathbf{l}^\perp)(\tfrac{1}{2}l^+r^- + \tfrac{1}{2}l^-r^+ - \mathbf{l}^\perp \cdot \mathbf{r}^\perp)(\tfrac{1}{2}r^+q^-) \,. \tag{5.47}$$

But (5.42)-(5.43) imply $|k^+l^-| > |k^-l^+|$ and $|l^+r^-| > |l^-r^+|$ while fig. 29 says that $\mathbf{k}^\perp \cdot \mathbf{l}^\perp$ and $\mathbf{l}^\perp \cdot \mathbf{r}^\perp$ are small, of order μ^2. So (5.47) scales like

$$\mu^{-8}(p^+k^-)(k^+l^-)(l^+r^-)(r^+q^-) \sim \mu^{-2} p \cdot q \tag{5.48}$$

since

$$k^-k^+ \sim l^-l^+ \sim r^-r^+ \sim \mu^2 \,, \tag{5.49}$$

which is the claimed result.

We are now in a position to estimate the size of diagrams such as fig. 24. It is useful to compare it directly to a "squared-tree" graph such as fig. 31 that likewise enters in at order g^4 in perturbation theory. Up to logarithms, fig. 31 scales like $g^4(E^2)^3$, with each of the three loop propagators contributing a factor of $E^2 \sim p \cdot q$ by Eq. (5.24). This is consistent with s multiplication along any of the three paths across the diagram. (We set the small energy scale μ^2 equal to unity and work with dimensionless energies for convenience.) In comparison, if in fig. 24 the momentum transfer s_1 across the first loop is of order E^2, then by s multiplication the momentum transfer s_2 across the second loop must be of order 1, so that the graph $\sim g^4(E^2)^2$, down by two powers of energy compared to the squared-tree graph. Alternatively, rather than taking

$s_1 \sim E^2$ and $s_2 \sim 1$, we can assign $s_1 \sim s_2 \sim E$ equally across both loops consistent with s multiplication, but this too gives g^4E^4.

Generalizing these arguments to arbitrary loop contributions to the propagator, we conclude that the bulk of the momentum transfer occurs where the graph can be cut to reveal the maximum number of lines. This means that at any *fixed* order in perturbation theory, the dominant diagrammatic contributions to the propagator as $p \cdot q \to \infty$ are precisely the squared-tree graphs discussed previously. But this observation, by itself, does not guarantee that graphs such as fig. 24 can be ignored. In fact, compared to the Ringwald approximation g^{-2} to the 2-point function (from two factors of $\phi_{\rm inst}$), the relative strength of fig. 24 is g^6E^4 which is of order $\alpha_{\rm w}^{-1}$ at sphaleron energies. So fig. 24 *might* be the first term in an exponential series that contributes to the holy grail function. On the other hand, perhaps it should be considered as a harmless $\mathcal{O}(\alpha_{\rm w})$ multiplicative correction to the squared-tree graph, fig. 23a. We recognize once again how delicate it is to extract the logarithm of an infinite series in which successive terms are of increasing importance.

5.4. Can the initial state be treated semiclassically? A one-loop miracle.

Let us admit the following: If a believable estimate for $\log \sigma_{\not B}$ requires an accurate evaluation of complicated multiloop diagrams, then the problem is hopeless, at least in the present approach. We close these Lectures on an optimistic note, an early hint that—despite the importance of loops—the hard line corrections, looked at in the right way, might nevertheless be treatable *semiclassically*, that is, by *tree graphs alone*. The result is due to Arnold, Mattis, McLerran and Yaffe.[60]

We begin in a journalistic mode, by quoting some formulae of Mueller's for pure $SU(2)$ gauge theory. Start with the n-point function in Ringwald approximation,

$$G^{(n)}_{\rm Ring} \;=\; A^{\mu_1 a_1}_{\rm inst}(p_1) \times \cdots \times A^{\mu_n a_n}_{\rm inst}(p_n)\,, \qquad (5.50)$$

with $A_{\rm inst}$ the Minkowski-continued instanton. We will assume as before that all the $p_i \cdot p_j$ are large, while the p_i^2 are small, close to, but for technical reasons

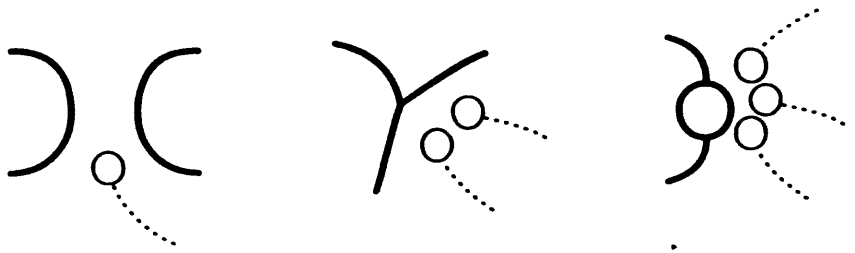

Fig. 32. The three $\mathcal{O}(\alpha^2)$ multiplicative corrections to fig. 21, from Ref. 40.

Fig. 33. The interpretation of fig. 32 as squared or cubed trees.

not exactly on, the mass shell. The order α correction to (5.50) consists of a single propagator insertion, as in fig. 22, and equals[39]

$$-\frac{\alpha\rho^2}{16\pi}\sum_{i,j=1}^{n} p_i\cdot p_j \log(-p_i\cdot p_j)\, G^{(n)}_{\rm Ring}\ , \tag{5.51}$$

neglecting terms of order $\alpha\cdot(p_i\cdot p_j)^0$. At order α^2 there are three types of corrections that come in, depicted in fig. 32a-c. (Also shown [fig. 33] is their interpretation as squared or cubed trees so the reader can see how they fit into the paradigm of Sec. 5.2.) These work out, respectively, to[40] *

$$\tfrac{1}{2}\Big(\frac{\alpha\rho^2}{16\pi}\Big)^2 \sum_{\substack{i,j,k,l=1\\ i,j,k,l\ \text{distinct}}}^{n} \big(p_i\cdot p_j\log(-p_i\cdot p_j)\big)\big(p_k\cdot p_l\log(-p_k\cdot p_l)\big)\, G^{(n)}_{\rm Ring}\ , \tag{5.52}$$

$$2\Big(\frac{\alpha\rho^2}{16\pi}\Big)^2 \sum_{\substack{i,j,k=1\\ i,j,k\ \text{distinct}}}^{n} \big(p_i\cdot p_j\log(-p_i\cdot p_j)\big)\big(p_i\cdot p_k\log(-p_i\cdot p_k)\big)\, G^{(n)}_{\rm Ring}\ , \tag{5.53}$$

and

$$\Big(\frac{\alpha\rho^2}{16\pi}\Big)^2 \sum_{\substack{i,j=1\\ i,j\ \text{distinct}}}^{n} \big(p_i\cdot p_j\log(-p_i\cdot p_j)\big)^2\, G^{(n)}_{\rm Ring}\ . \tag{5.54}$$

In Eqs. (5.52)-(5.54), terms that are of order $\alpha^2 p_i\cdot p_j$ have been dropped. Adding these three expressions gives for the total order α^2 result,

$$\frac{1}{2!}\Big(\frac{\alpha\rho^2}{16\pi}\Big)^2\Big(\sum_{i,j=1}^{n} p_i\cdot p_j\log(-p_i\cdot p_j)\Big)^2\, G^{(n)}_{\rm Ring}\ . \tag{5.55}$$

Notice that Eq. (5.55) has exactly the form required to be part of an exponential series begun by Eq. (5.51). The important point in the above formulae is that loops and trees conspire to give a simple result.

* We take this occasion to correct some minor misprints in Eqs. 28-30 of Ref. [40]. Mueller's formulae contain additional pieces but these vanish when momentum conservation is imposed, so we omit them for simplicity. However, the result of Ref. [60] discussed below holds for these omitted terms as well.

Now let us repeat this calculation in a different, and seemingly more awkward way, using an effective action approach.[60] We evaluate the n-point function

$$\int \mathcal{D}A\, A^{\mu_1 a_1}(p_1)\cdots A^{\mu_n a_n}(p_n)\, e^{iS[A]} \tag{5.56}$$

by splitting the fields into classical and fluctuating components, and making the replacement

$$A^{\mu_i a_i}(p_i) \;=\; A^{\mu_i a_i}_{\rm inst}(p_i) \;+\; \delta A^{\mu_i a_i}(p_i) \;=\; A^{\mu_i a_i}_{\rm inst}(p_i)\,\exp\log\left(1+\frac{\delta A^{\mu_i a_i}(p_i)}{A^{\mu_i a_i}_{\rm inst}(p_i)}\right)\ . \tag{5.57}$$

Taylor expanding the logarithms then leads to an infinite number of new interaction vertices which we shall denote graphically by thick blobs. Other vertices come from the usual action $S[A]$ which we likewise expand about $A_{\rm inst}$. Note that unlike usual vertices, m-point blobs $\sim g^m$ from $(A_{\rm inst})^{-m}$. Another difference is that blobs are real whereas the usual vertices come with the standard factor of i attached. Evaluating the n-point function (5.56) now becomes equivalent to calculating the effective action in the presence of the new interactions generated by

$$\sum_{i=1}^{n}\log\left(1+\frac{\delta A^{\mu_i a_i}(p_i)}{A^{\mu_i a_i}_{\rm inst}(p_i)}\right)\ . \tag{5.58}$$

The order α and α^2 contributions to the effective action are pictured in fig. 34 and fig. 35, respectively.

Of course, if carried out *exactly*, both calculational methods must precisely agree. The nontrivial observation is this:[60] If, following Mueller, one only works to leading order in energy, throwing out terms of order $\alpha(p_i\cdot p_j)^0$ and $\alpha^2 p_i\cdot p_j$, then in the effective action approach Eqs. (5.51) and (5.55) are reproduced by the *tree graphs alone*, figs. 34a, 35a and b. Equivalently, the loop contributions to the effective action all cancel to these orders. The diligent reader should have no trouble verifying either claim with the use of Eqs. (5.52)-(5.54).

In conclusion, *if* this loop cancellation persists to all orders, and *if* it is understood how best to couple the initial hard quanta to the soft high-multiplicity final state, and *if* at the same time the effect of phase space can be incorporated

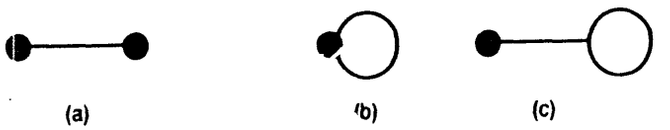

Fig. 34. The $\mathcal{O}(\alpha\ )$ contributions in the effective action approach.[60] Thick blob vertices come from the effective interaction (5.58).

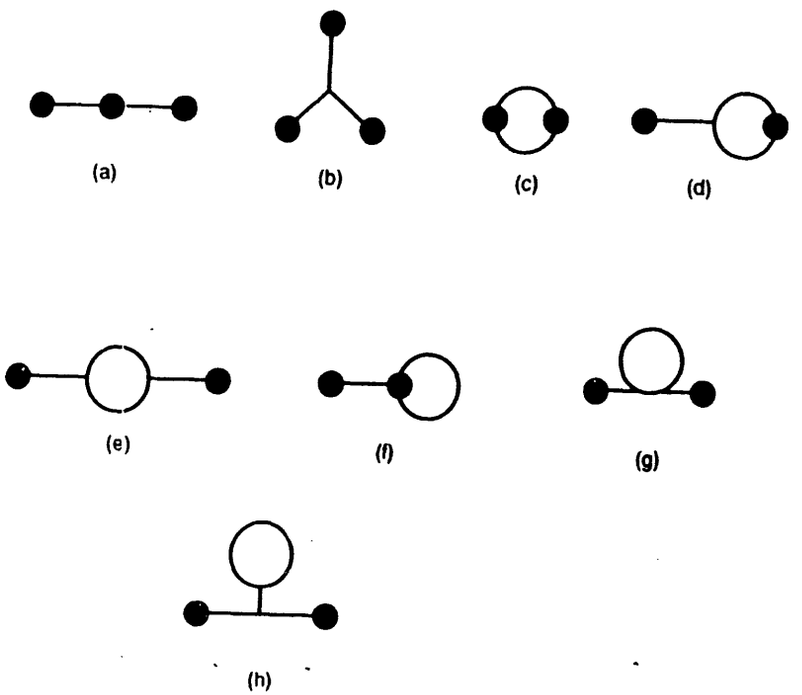

Fig. 35. The $\mathcal{O}(\alpha^2\ )$ contributions in the effective action approach.[60] Diagrams containing only one blob have not been displayed, since they cannot produce large dot products $p_i \cdot p_j$, $i \neq j$, of external momenta, and so are necessarily subleading in energy.

through the R-term or valley method, and *if* the appropriate boundary conditions can be formulated, and *if* multiinstanton contributions can be neglected—then indeed the calculation of $\log \sigma_{\not B}$ will have been reduced to solving a classical equation, and the riddle of high-energy baryon number violation will at last be answered.

References

[1] A. Ringwald, *Nucl. Phys.* **B330**, 1 (1990).

[2] O. Espinosa, *Nucl. Phys.* **B343**, 310 (1990). This was the first correct treatment of the global isospin collective coordinates in the context of B violation.

[3] H. Goldberg, *Phys. Lett.* **B246**, 445 (1990), and contribution to Ref. [9].

[4] J. Cornwall, *Phys. Lett.* **B243**, 271 (1990), and contribution to Ref. [9].

[5] V. Zakharov, Max Planck preprint MPI-PAE/PTh 91-11 (1991).

[6] M. Maggiore and M. Shifman, TPI preprints TPI-MINN-91/17-T and 91/21-T (1991).

[7] T. Lee and A. Mueller, Columbia preprint CU-TP-523 (1991).

[8] N. Manton, *Phys. Rev.* **D28**, 2019 (1983); F. Klinkhamer and N. Manton, *Phys. Rev.* **D30**, 2212 (1984).

[9] For a wide range of approaches to this question, see *Baryon Number Violation at the SSC? Proceedings of the Santa Fe Workshop*, eds. M. Mattis and E. Mottola, Singapore, World Scientific, 1990.

[10] S. Coleman, *The Uses of Instantons*, in the Proceedings of the 1977 Erice Summer School, ed. A. Zichichi; reprinted in S. Coleman, *Aspects of Symmetry*, Cambridge Univ. Press 1985.

[11] M. Voloshin, TPI preprint TPI-MINN-91/19-T (1991).

[12] G. 't Hooft, *Phys. Rev.* **D14**, 3432 (1976); **D18**, 2199(E) (1978).

[13] S. Adler, *Phys. Rev.* **177**, 2426 (1969); J. Bell and R. Jackiw, *Nuovo Cim.* **60A**, 47 (1969).

[14] G. Abrams, *et al.* , *Phys. Rev. Lett.* **63**, 2173 (1989).

[15] A. Belavin, A. Polyakov, A. Schwartz and Y. Tyupkin, *Phys. Lett.* **B59**, 85 (1975).

[16] D. Gross, R. Pisarski and L. Yaffe, *Rev. Mod. Phys.* **53**, 43 (1981).

[17] S. Khlebnikov, V. Rubakov and P. Tinyakov, DESY preprint DESY-91-033 (1991). Here it is shown that periodic instantons have nothing to do with the problem of high-energy B violation.

[18] V. Kuzmin, V. Rubakov and M. Shaposhnikov, *Phys. Lett.* **155B**, 36 (1985).

[19] P. Arnold and L. McLerran, *Phys. Rev.* **D36**, 581 (1987); *ibid.*, **D37**, 1020 (1988).

[20] For recent reviews of the related problem of anomalous B violation at high temperatures, see M. Shaposhnikov (this volume); P. Arnold, Proceedings of the 1990 TASI Summer School; E. Mottola, Proceedings of the 1989 TASI Summer School.

[21] I. Affleck, *Nucl. Phys.* **B191**, 445 (1981).

[22] L. McLerran, A. Vainshtein and M. Voloshin, *Phys. Rev.* **D42**, 171 (1990).

[23] G. Farrar and R. Meng, *Phys. Rev. Lett.* **65**, 3377 (1990).

[24] A. Ringwald, in Ref. [9].

[25] P. Arnold and M. Mattis, *Phys. Rev. Lett.* **66**, 13 (1991).

[26] V. V. Khoze and A. Ringwald, *Nucl. Phys.* **B355** 351 (1991).

[27] V. V. Khoze and A. Ringwald, *Phys. Lett.* **B259** 106 (1991).

[28] T. Banks, G. Farrar, M. Dine, D. Kaxabali, B. Sakita, *Nucl. Phys.* **B347**, 581 (1990), and in Ref. [9].

[29] X. Li, L. McLerran, M. Voloshin and R. Wang, TPI preprint TPI-MINN-91/16-T (1991).

[30] R. Cutkosky, *J. Math. Phys.* **1**, 429 (1960). The clearest introduction to cutting rules is G. 't Hooft and T. Veltman, *Diagrammar*, pp. 210-217, in D. Speiser *et al.* , eds., *Particle Interations at Very High Energies*, Part B (1974).

[31] V. Zakharov, TPI preprint TPI-MINN-90/7-T.

[32] L. McLerran, A. Vainshtein and M. Voloshin, *Phys. Rev.* **D42**, 180 (1990).

[33] P. Arnold and M. Mattis, *Phys. Rev.* **D42**, 1738 (1990) and Ref. [9].

[34] L. Yaffe, in Ref. [9].

[35] S. Khlebnikov, V. Rubakov and P. Tinyakov, *Nucl. Phys.* **B350**, 441 (1991).

[36] P. Arnold and M. Mattis, Los Alamos preprint LA-UR-91-1858 (1991).

[37] L. Brown, R. Carlitz, D. Creamer and C. Lee, *Phys. Rev.* **D17**, 1583 (1978).

[38] H. Levine and L. Yaffe, *Phys. Rev.* **D19**, 1225 (1979).

[39] A. Mueller, *Nucl. Phys.* **B348**, 310 (1991).

[40] A. Mueller, *Nucl. Phys.* **B353**, 44 (1991).

[41] Z. Bern, private communication.

[42] See for example Sec. III.3 of P. Ramond, *Field Theory: A Modern Primer*, Benjamin Cummings, 1981.

[43] M. Porrati, *Nucl. Phys.* **B347**, 371 (1990).

[44] D. Diakonov and V. Petrov, in the Proceedings of the 26th Winter School of the Leningrad Institute of Nuclear Physics, Leningrad 1991 (in Russian).

[45] A. Mueller, Columbia preprint CU-TP-512 (1991).

[46] P. Arnold and M. Mattis, *Mod. Phys. Lett.* **A6**, 2059 (1991).
[47] D. Diakonov and M. Polyakov, Leningrad LNPI preprint (1991).
[48] V. V. Khoze and A. Ringwald, CERN preprint CERN-TH-6082/91 (1991).
[49] For a recent review focusing on the use of the valley method in high-energy scattering, see A. Ringwald, Proceedings of the 1991 PASCOS meeting.
[50] I. Balitsky and A. Yung, *Phys. Lett.* **168B**, 113 (1986).
[51] A. Yung, *Nucl. Phys.* **B297**, 47 (1988).
[52] J. Verbaarschot, SUNY preprint SUNY-NTG-91/7 (1991).
[53] R. Jackiw and C. Rebbi, *Phys. Rev.* **D14**, 517 (1976).
[54] H. Aoyama and H. Kikuchi, *Phys. Lett.* B247, 75 (1990); *Phys. Rev.* **D43**, 1999 (1991).
[55] V. Zakharov, *Nucl. Phys.* **B353**, 683 (1991).
[56] M. Maggiore and M. Shifman, TPI preprint TPI-MINN-91/24-T (1991).
[57] M. Shifman, A. Vainshtein and V. Zakharov, *Nucl. Phys.* **B165**, 45 (1980); V. Novikov, M. Shifman, A. Vainshtein and V. Zakharov, *Sov. Phys. Usp.* **25**, 195 (1982).
[58] E. Shuryak, *Nucl. Phys.* **B203**, 93, 116, 140 (1982).
[59] S. Khlebnikov and P. Tinyakov, CERN preprint CERN-TH.6146/91, to appear in Phys. Lett. B.
[60] P. Arnold, M. Mattis, L. McLerran and L. Yaffe, in progress.
[61] S. Khlebnikov, V. Rubakov and P. Tinyakov, *Nucl. Phys.* **B347**, 783 (1990).

END

DATE FILMED

10/29/91